

THE TARGETS OF OPPORTUNITY SOURCE CATALOG, PRIORITIZATION, SCHEDULER AND
RELATED MECHANICS FOR THE EUSO-SPB2 MISSION

by
Hannah Wistrand

© Copyright by Hannah Wistrand, 2024

All Rights Reserved

A thesis submitted to the Faculty and the Board of Trustees of the Colorado School of Mines in partial fulfillment of the requirements for the degree of Master of Science (Applied Physics).

Golden, Colorado

Date _____

Signed: _____

Hannah Wistrand

Signed: _____

Dr. Lawrence Wiencke
Thesis Advisor

Golden, Colorado

Date _____

Signed: _____

Dr. Fred Sarazin
Professor and Department Head
Department of Physics

ABSTRACT

The Extreme Universe Space Observatory on a Super Pressure Balloon 2 (EUSO-SPB2) was developed to observe ultra high energy cosmic rays and very high energy (VHE) neutrinos from suborbital space. These earth-skimming VHE tau-neutrinos can interact with the Earth's limb to produce tau leptons which can exit the Earth and decay to initiate extensive air showers (EASs). Below PeV energies, ground-based detectors such as IceCube and ANTARES have utilized km^3 -scale mediums to observe these EASs via their optical Cherenkov emissions. However, at higher energies, much of the sky becomes inaccessible to ground-based detectors because of Earth attenuation effects. As the interest in these multi-messenger particles increases, the development of space-based detectors is ongoing. EUSO-SPB2 was launched on May 13th, 2023 from Wanaka, NZ on a high-altitude balloon with a state-of-the-art Cherenkov Telescope (CT) which pioneered a solution to the attenuation problem and had the ability to respond in real-time to potential neutrino alerts throughout the sky. When the CT was pointed below the limb, the mission of the EUSO-SPB2 Targets of Opportunity (ToO) program was to follow up on astrophysical transient source alerts and selected steady state sources by searching for upward-going optical Cherenkov emission from PeV-scale EASs induced by tau neutrinos. To do this, a software program that collects ToO alerts from several online databases, sorts through these alerts, prioritizes and schedules them was developed alongside a mechanical system to point the CT. The flight lasted 1 day, 12 hours and 53 minutes. This short flight did not allow for ample time to test the prepared ToO software or to point the CT at a ToO. Studies are currently ongoing to test this software with data from longer balloon flights. These follow-up mechanisms utilized by the CT to view ToOs are the subject of this thesis.

TABLE OF CONTENTS

ABSTRACT	iii
LIST OF FIGURES	vi
LIST OF TABLES	viii
ACKNOWLEDGMENTS	ix
DEDICATION	x
CHAPTER 1 INTRODUCTION	1
CHAPTER 2 BACKGROUND	2
2.1 Why Neutrinos?	2
2.2 Neutrino Detection - Previous Work	3
2.3 EUSO-SPB2 Goals	8
CHAPTER 3 THE EUSO-SPB2 TARGETS OF OPPORTUNITY	10
3.1 Sources of Interest	10
3.2 ToO Catalog	11
3.3 ToO Prioritization	14
3.3.1 A Note on Gravitational Waves	15
CHAPTER 4 THE EUSO-SPB2 TOO FOLLOW-UP MECHANISMS	17
4.1 ToO User Interface	17
4.2 ToO Schedule Creation	20
4.3 Shutter/Tilt System	22
4.3.1 The PLC Box	23
4.3.2 The Tilt System	24
4.3.3 Calibration and Testing of the Tilt System	25
4.3.4 The Shutter System	29
4.3.5 Calibration and Testing of the Shutter System	29
CHAPTER 5 PERFORMANCE RESULTS	32

5.1	Shutter/Tilt Performance	32
5.2	ToO Performance	34
	CHAPTER 6 LONG DURATION FLIGHT STUDY	39
	CHAPTER 7 CONCLUSION	43
	REFERENCES	44
	APPENDIX A SHUTTER TILT SYSTEM OPERATION MANUAL	48
A.1	Commanding	48
A.1.1	Timing of the ST	49
A.2	Status Package	49
A.2.1	Grafana User Interface	49
A.2.2	Command Line	49
A.3	Troubleshooting and Expert Information	50
A.3.1	Expert Commands	51
A.3.2	Limits	51
A.3.3	"Full Status" and Device Configuration	51
A.3.4	Status Bytes	51
A.3.5	System Specs	51
	APPENDIX B ALL SOURCES OBSERVABLE ON MAY 14TH, 2023	56

LIST OF FIGURES

Figure 2.1	Measured and expected fluxes of natural and nuclear-reactor neutrinos	5
Figure 2.2	IceCube was the first a ground-based neutrino detector of its kind, constructed in 2010 . . .	6
Figure 2.3	Plot of the recorded and expected sensitivities of discussed neutrino detectors, including EUSO-SPB2, POEMMA, IceCube, IceCube Gen2, and ANTARES.	8
Figure 2.4	With its Cherenkov telescope, EUSO-SPB2 aims to observe cosmic rays via the Direct Cherenkov Technique when pointed above the limb. Below the limb, EUSO-SPB2 searched for upwards-going air showers induced by tau-neutrinos.	8
Figure 2.5	Illustration of the Earth-skimming method used for neutrino detection.	9
Figure 3.1	Artist representations of some of the types of sources of interest to the EUSO-SPB2 targets of opportunity program.	11
Figure 4.1	Step by step of the ToO scheduling software from receiving the alerts to scheduling ToOs for observation.	17
Figure 4.2	The user interface for the ToO scheduler.	18
Figure 4.3	The user interface for adding single sources to the ToO database and scheduler.	19
Figure 4.4	An example skymap visualization (in galactic coordinates) for all possible observable sources for the night of May 14, 2023.	20
Figure 4.5	Flowchart of the ToO scheduling process.	21
Figure 4.6	ToO trajectories in the CT field of view	21
Figure 4.7	Field of view of the EUSO-SPB2 Cherenkov detector.	22
Figure 4.8	A rendering of the fully configured EUSO-SPB2 detector	23
Figure 4.9	Internal view of the PLC Box that housed the communicative portion of the ST system. . .	23
Figure 4.10	Assembled tilt mechanism.	24
Figure 4.11	Flowchart of the tilt operation	25
Figure 4.12	The setup for calibration of the inclinometers.	26
Figure 4.13	The resulting calibration curve for the GSE inclinometer.	26
Figure 4.14	The calibration curve resulting from rigorous testing of the tilt mechanism.	27
Figure 4.15	The uncertainty caused by the conversion equation between the voltage received by the PLC from the GSE inclinometer and the angle reported to the operator.	28

Figure 4.16	The inclinometer in its final location atop the CT frame, directly behind the top shutter mechanism.	28
Figure 4.17	Top view of the shutter mechanisms.	29
Figure 4.18	Side view of the shutter mechanisms.	30
Figure 4.19	Flow chart of the shutter operation.	30
Figure 4.20	Limit switch used to stop each shutter from opening or closing too far.	31
Figure 5.1	Plot of the altitude of the super pressure balloon carrying EUSO-SPB2 from 00:02 UTC May 13, 2023 to 12:54 UTC May 14, 2023.	32
Figure 5.2	Plot of the uncertainty of the tilt mechanism over the duration of the EUSO-SPB2 flight.	33
Figure 5.3	Shutter operation for night 1 of the EUSO-SPB2 flight.	34
Figure 5.4	Shutter operation for night 2 of the EUSO-SPB2 flight.	35
Figure 5.5	Out of the 102-source database, 5 sources were scheduled for night two of EUSO-SPB2 operations.	36
Figure 5.6	There were 8 sources that were not scheduled due to repeating priority values.	37
Figure 6.1	In order to further test the ToO software, a simulation was run on the SuperBIT trajectory.	39
Figure 6.2	Over the span of 39 days, an average of 2-3 sources were scheduled each night.	40
Figure 6.3	There was a total of 14 unique sources that showed up over the 39 nights.	41
Figure 6.4	The most frequently scheduled sources were AT 2023clx and MG2 J144640+3110, being scheduled on a total of 22 out of the 39 nights.	41
Figure A.1	The ST manual welcome prompt	48
Figure A.2	ST user commands	48
Figure A.3	Grafana user interface	49
Figure A.4	ST status message	50
Figure A.5	ST expert commands	51
Figure A.6	Shutter stepper motor specs	54
Figure A.7	Shutter stepper motor specs	55
Figure B.1	All the sources in the ToO source catalog the night of May 14th 2023	57

LIST OF TABLES

Table 3.1	Part 1 of the complete list of steady sources included in the ToO source catalog for May 14, 2023. These sources are never removed from the catalog.	12
Table 3.2	Part 2 of the complete list of steady sources included in the ToO source catalog for May 14, 2023. These sources are never removed from the catalog.	13
Table 3.3	The list of ToO sources of interest and their respective priority values as assigned for the EUSO-SPB2 mission.	14
Table 4.1	Schedule produced by the software for May 14, 2023.	22
Table 6.1	The number of alerts the GCN received for each GCN-registered observatory from February 1, 2023 to May 25, 2023.	42
Table A.1	Timing of the ST	49
Table A.2	ST status headers	50
Table A.3	ST limits	51
Table A.4	Device configuration status	52
Table A.5	Status message	53
Table A.6	System specs	54

ACKNOWLEDGMENTS

I would like to thank and acknowledge Dr. Lawrence Wiencke, Dr. Mary Hall Reno, the EUSO-SPB2 collaboration, and my wonderfully enthusiastic friends and family for their guidance and support throughout this process. I would not be the person I am today, or the scientist behind this thesis without every one of these individuals. Also a special thank you to my brother, Kyle Wistrand, who has always supported my scientific endeavors and helped show me the ropes of coding, and to my high school physics teacher, Dr. Nate Macon, from whom I learned that there is outstanding beauty in physics - so long as you stay curious. Thank you.

For those that shall follow after.

CHAPTER 1

INTRODUCTION

The Extreme Universe Space Observatory on a Super Pressure Balloon 2 (EUSO-SPB2) was developed to observe ultra high energy cosmic rays and very high energy (VHE) neutrinos from suborbital space [1]. These Earth-skimming VHE tau-neutrinos can interact with the Earth's limb to produce tau leptons which can exit the Earth and decay to initiate extensive air showers (EASs). These EASs can then be observed via their optical Cherenkov emissions.

Below PeV energies, ground-based detectors such as IceCube and ANTARES have utilized km^3 -scale mediums with the water Cherenkov technique and relied on their sky coverage to increase the likelihood of detecting a neutrino source. However, at higher energies, much of the sky becomes inaccessible to ground-based detectors because of Earth attenuation effects. As the interest in these multi-messenger particles increases, the development of space-based detectors is ongoing. EUSO-SPB2 pioneers a solution to the attenuation problem while overcoming a restricted field of view as a pathfinder to a space-based detector such as the Probe of Extreme Multi-Messenger Astrophysics (POEMMA) [2] with the ability to respond to potential neutrino alerts throughout the sky.

EUSO-SPB2 features two 1m diameter aperture telescopes carried as the payload on a Super Pressure Balloon. The Fluorescence Telescope (FT), which points down, records fluorescence light from cosmic ray EASs with energies above 1 EeV. The Cherenkov Telescope (CT) features a silicon photomultiplier camera system that points near the Earth's limb [3, 4]. Below the limb, the CT follows up on astrophysical transient source alerts and selected steady state sources by searching for upward-going optical Cherenkov emission from PeV-scale EASs induced by tau neutrinos. These sources that pass into the CT field of view are called Targets of Opportunity (ToO). The follow-up mechanisms utilized by the CT to view these ToOs are the subject of this thesis.

CHAPTER 2

BACKGROUND

The EUSO-SPB2 CT aims to observe PeV-scale EASs induced by tau neutrinos from astrophysical sources. This investigation is intended to both verify the observation method, set limits, and to possibly observe a neutrino from a very bright nearby transient source.

2.1 Why Neutrinos?

Neutrinos are informative messengers, virtually unaffected by external forces after leaving their origin. They are undeflected by extra-galactic magnetic fields and unattenuated in the photon-filled universe. Astrophysical neutrinos play an important role as information carriers for hard-to-identify and extremely distant, high-energy cosmic accelerators. There is also reason to believe they may provide direct evidence of the highest-energy cosmic-ray sources.

There exist a few categories of neutrinos, depending on their production mechanisms. Solar neutrinos make up the largest portion of the neutrino flux that the Earth experiences. The theory driving our understanding of solar neutrinos, stellar nucleosynthesis, poses that the Sun produces neutrinos through nuclear fusion. The Sun produces only electron-neutrinos (ν_e) through this mechanism, though neutrino oscillation may occur to change these electron-neutrinos to muon- (ν_μ or even tau- (ν_τ)) neutrinos by the time they hit Earth [5]. Successful solar neutrino detection has paved the way for research reliant on this and other types of neutrinos. Decades of solar neutrino experiments such as GALLEX/GNO [6] and SAGE [7], and water Cherenkov detectors such as Kamiokande [8], Super-Kamiokande [9], and SNO [10] have been making observations since the 1960s, aiding in our understanding of the Sun and leading to the discovery of neutrino masses. These neutrino masses are promising in the realm of new physics topics such as dark matter [5] and as messengers for the astrophysical community as discussed in this thesis.

Astrophysical neutrinos can be created through the interaction of cosmic rays in astrophysical sources (see sources of interest) and are a little tougher to detect. Neutrinos can be produced as decay products of secondary pion/meson decays that are typically created in proton-proton interactions. The proton-proton interaction produces a pion (π^+) and a meson (π^-), which decay to an electron, neutrino and antineutrino. These different production mechanisms result in three different types (flavors) of neutrinos - the electron-, the muon-, and the tau-neutrino [11].

The abundance of each flavor varies across the differing production mechanisms. For example, the canonical expectation for neutrino flavors at astrophysical sources is a 2:1:0 ratio between muon-, electron-,

and tau-neutrinos produced through the full-pion decay mechanism. In this instance, the pion resulting from a cosmic ray interaction with a proton produces a muon μ and a muon-neutrino ν_μ . The muon then decays to a muon-neutrino, an electron e^- , and an electron-neutrino ν_e [11].

$$\pi^+ = \mu^+ + \nu_\mu \quad (2.1)$$

$$\mu^+ = \bar{\nu}_\mu + e^+ + \nu_e \quad (2.2)$$

Other ratios exist, namely through muon damping (1:0:0) and neutron decay (0:1:0), but they are much less likely than the pion decay scenario [11]. The muon damping mechanism may reveal information regarding the magnetic field strength of astrophysical sources. This identification may be possible with IceCube-Gen2 if the mechanism results from a transition from the full pion mechanism at PeV energies. This is beyond the scope of this thesis, but more information on these less abundant neutrino ratios can be found in [11].

When the 2:1:0 ratio due to the full-pion mechanism undergoes oscillatory effects (where one flavor may change to another), by the time astrophysical neutrinos reach the Earth's atmosphere, there is approximately a 1:1:1 ratio between the three flavors [11, 12]. These neutrinos go on to either initiate extensive air showers (EASs) or produce detectable leptons when they interact with the nucleons of the atmospheric particles. The tau-lepton is a product of the interaction of a tau-neutrino as it is attenuated by the Earth. The lepton, l , typically takes approximately 80% of the neutrino energy, while the rest goes into a hadronic component, X , of lower energy:

$$\nu_\tau + N = l_\tau + X \quad (2.3)$$

This lower energy hadronic component immediately produces a low energy shower that does not leave the Earth, but the tau-lepton continues to propagate through the atmosphere until it decays, producing another air shower of higher energy [13].

The tau-neutrino is the subject of the EUSO-SPB2 neutrino search through the Targets of Opportunity mechanism. The EUSO-SPB2 CT, with the help of a tilting mechanism, is able to point above and below the Earth's limb. It is when the CT is pointed below the limb that these tau-neutrino EASs are in the field of view. When the CT is pointed above the limb, the search is for ultra high energy cosmic rays which interact with atmospheric particles to produce EASs.

2.2 Neutrino Detection - Previous Work

Detecting these neutrinos is challenging and EUSO-SPB2 is by no means the first experiment to try. However, EUSO-SPB2 is one of the first experiments to attempt high altitude-based detection. Neutrinos

have extremely small interaction cross sections and although this cross section increases with energy, astrophysical neutrino emissions are expected to follow steeply falling power laws for which the rising cross section cannot compensate [12]. The resulting low flux level in the TeV-PeV energy range prompted the construction of kilometer-scale neutrino detectors which utilize volumetric arrays of light sensors such as photomultiplier tubes (PMTs) and which rely on large natural bodies of water such as a deep lake, sea or glacial ice to be economically feasible [13]. The instruments detect Cherenkov photons emitted by extensive air showers initiated by neutrino interactions in the Earth's limb.

Since the 1950s, low-energy neutrinos have been the subject of astrophysical neutrino detection success. After the first detection of neutrinos from a nuclear reactor in 1956 [14], solar neutrino detection in 1968 [15] and neutrinos detected from Supernova SN 1987A [16] in 1987 guided the field for decades. These detectable neutrinos dominate the keV to MeV range. On the μeV and meV range, cosmological (relic) neutrinos, exist, though their detection remains just out of reach since their reaction cross section and interaction energies are frustratingly small [17]. Atmospheric neutrinos, created in cosmic ray interactions in the Earth's atmosphere, were first detected by the Kolar Gold Fields experiment in 1965 [18] and make up the MeV to PeV range. The highest-energy neutrinos, astrophysical (cosmic) neutrinos, are the subject of this thesis, and exist in the PeV and above energy range. These neutrino types and their respective energies are shown in Figure 2.1.

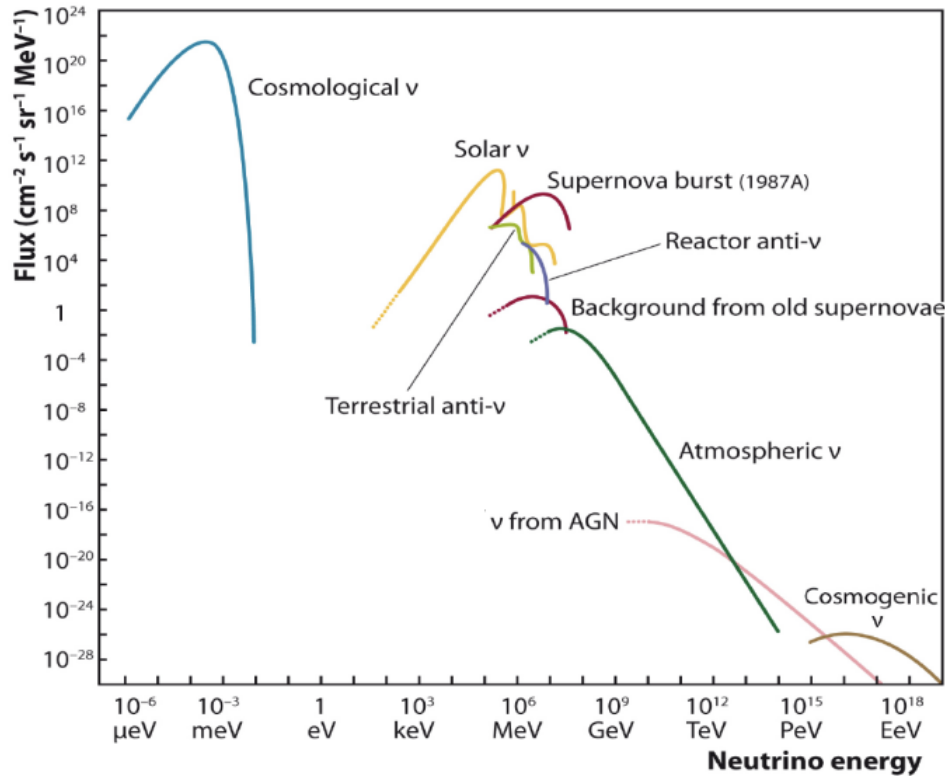


Figure 2.1 Measured and expected fluxes of natural and nuclear-reactor neutrinos. The energy range from keV to several GeV is covered by solar neutrinos and is the domain of underground detectors. The region from tens of GeV to about 100 PeV, is the domain of atmospheric neutrinos and is addressed by Cherenkov light detectors underwater and in ice. The highest energies are only accessible with huge detector volumes and methods described below [17].

To date, two ground-based detectors, IceCube [19] and ANTARES [20], have been successful at high-energy neutrino detection with a sensitivity to all flavors. These detectors utilize the physics of the weak interactions of neutrinos and analyze the energy losses of the secondary particles they produce to determine neutrino flavor. IceCube, shown in Figure 2.2, is currently the most sensitive high-energy neutrino detector and is deployed in the deep Antarctic ice near the South Pole. IceCube is sensitive to all neutrino flavors through varying detection techniques. IceCube is most sensitive to muon-neutrinos, which make track like signatures when they collide with the detector’s ice, leaving a straight line of light signals in its wake. Electron-neutrinos typically scatter several times before losing enough energy to fall below the Cherenkov threshold which results in detectable events that are more spherical, or ”cascade”-like, rather than the ”track”-like muon-neutrino events. IceCube searches for tau-neutrinos by looking for the 2 signals from the double-decay process as described in Equation 2.3 on page 3, where a cascade is seen both at the tau-lepton creation and decay. In 2013, IceCube recorded the first observation of emission of astrophysical

neutrinos in the TeV to PeV energy range [21, 22].

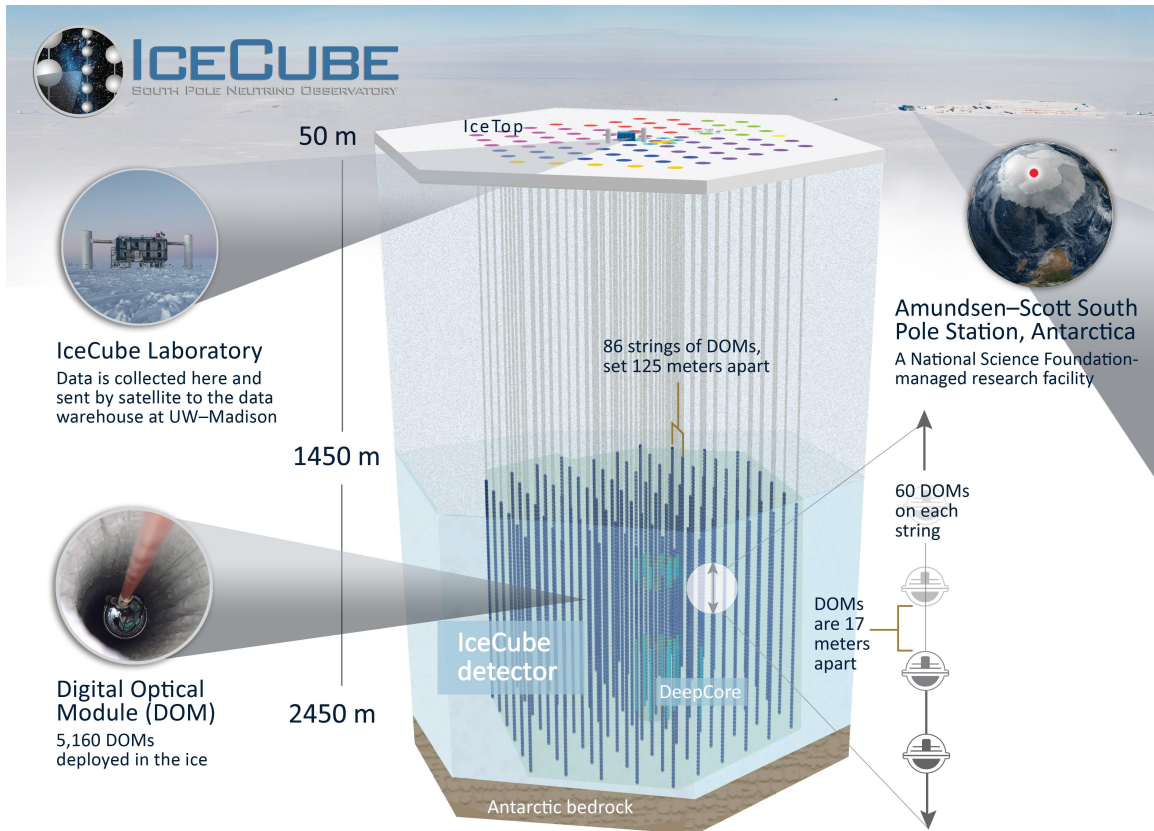


Figure 2.2 IceCube was the first a ground-based neutrino detector of its kind, constructed in 2010. In 2013, IceCube recorded the first observation of emission of astrophysical neutrinos in the TeV to PeV energy range. The detector consists of 2 parts - a surface array, IceTop, and a denser inner subdetector, DeepCore. Below the ice, IceCube consists of 5,160 digital optical modules (DOMs), each with a ten-inch photomultiplier tube and associated electronics. The DOMs are arrayed over a cubic kilometer from 1,450 meters to 2,450 meters depth [21]

In correlating these detections to their point-sources of origin, there are a couple options. IceCube and ANTARES either analyze source locations one at a time, or stack sources belonging to the same catalog class to look for correlations simultaneously. They then further divide these analyses between time-dependent and time-integrated searches [13]. While these processes have yielded promising results [23–25] for the field of high-energy neutrino detection (see the section of sources of interest for more information on successful detection), the correlation process is furthered by a multi-messenger approach [13]. IceCube and ANTARES issue real time alerts to the astronomical community when high-energy neutrino events of likely astrophysical origin are recorded in the detector [26]. Other detectors are then able to follow-up on these alerts to correlate neutrino signals in space and time with other signals from

photons, x-rays, gamma-rays or gravitational waves, which in turn improves the overall sensitivity to joint emitters of astrophysical neutrinos.

Neutrino detection is thus an inherently collaborative field. As sensitivity of one instrument improves, the others are forced to push their limits to both compete with this new threshold and to support the potential of the improved instrument. Some of these improvements may include increasing data collection through the construction of additional neutrino telescopes (or the expansion of existing ones), improving angular resolution of detectors and further integrating current neutrino telescopes with the multi-messenger astronomy (MMA) community. The increase in data collection is a goal of next-generation instruments such as IceCube-Gen2. Additional sensitivity will be provided by KM3NeT-ARCA [27], Baikal-GVD [28], and the recently-proposed P-ONE telescope [29] which are expected to reach the km³-scale in the coming decade.

However, several issues still remain. As neutrino energy increases, the Earth becomes opaque as neutrino absorption in the Earth becomes significant. This reduces the sensitivity of current detectors to these neutrinos that pass through the Earth to reach the detector [12, 30]. Additionally, a high muon background for down-going neutrinos means that these issues combine to reduce the peak sensitivity for high energy neutrino telescopes to near the local horizon [13]. For detectors placed near the Earth's equator, like KM3NeT and GVD, this means that the region of maximum instantaneous sensitivity sweeps the sky as the Earth rotates, while for equatorially offset detectors like IceCube and IceCube-Gen2, sensitivity will remain near the celestial equator for less than PeV-scale neutrinos.

Target of opportunity (ToO) observations - long-term monitoring programs - may provide temporal coverage over different timescales for a collection of sources across the sky, a step towards resolving these issues and improving correlation studies over the whole sky.

2.3 EUSO-SPB2 Goals

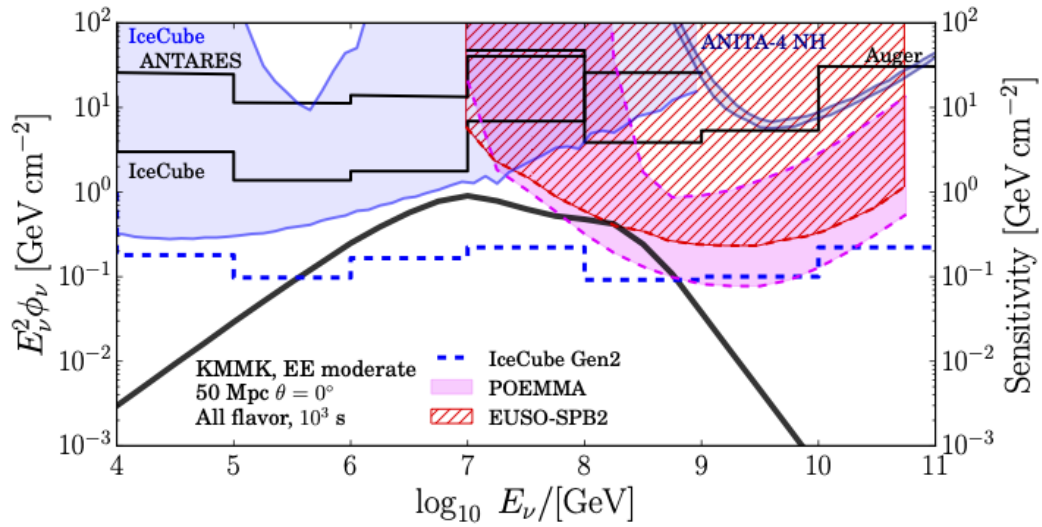


Figure 2.3 Plot of the recorded and expected sensitivities of discussed neutrino detectors, including EUSO-SPB2, POEMMA, IceCube, IceCube Gen2, and ANTARES. As seen here, EUSO-SPB2 aims for a higher sensitivity of VHE neutrinos than IceCube and IceCube Gen2, and bridging the sensitivity gap between IceCube (both generations) and detectors such as ANITA-4 NH and ANTARES.

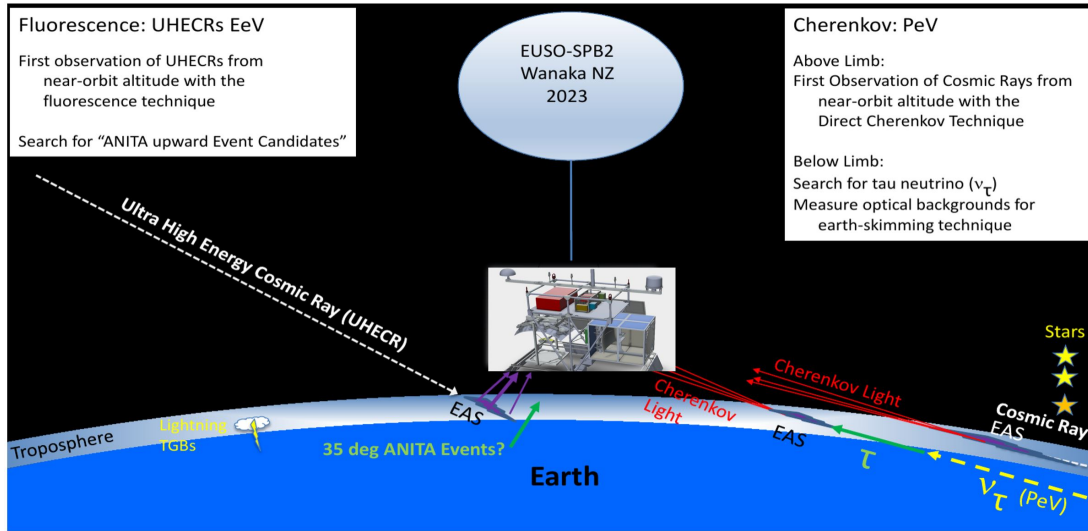


Figure 2.4 With its Cherenkov telescope, EUSO-SPB2 aims to observe cosmic rays via the Direct Cherenkov Technique when pointed above the limb. Below the limb, EUSO-SPB2 searched for upwards-going air showers induced by tau-neutrinos.

EUSO-SPB2 aims to assist in the correlation process with a sensitivity to very high energy (VHE) tau neutrinos above 10PeV, as shown in Figure 2.3. As described in Figure 2.4, the EUSO-SPB2 CT aims to observe Cherenkov light from extensive air showers initiated by cosmic rays, measure the background

conditions for the detection of neutrino induced upwards going air showers and search for neutrinos from astrophysical transient events. When the detector is pointed above the Earth's limb, the CT searches for ultra-high-energy (UHE) cosmic rays which interact with the particles in the atmosphere to produce extensive air showers. When the detector is pointed below the Earth's limb, the search is for very-high-energy (VHE) tau-neutrinos which have traveled through the Earth's layers, decayed to tau leptons and then interacted with the particles in the atmosphere to produce detectable extensive air showers (see Figure 2.5). The search for neutrinos from astrophysical transient events is the focus of this paper.

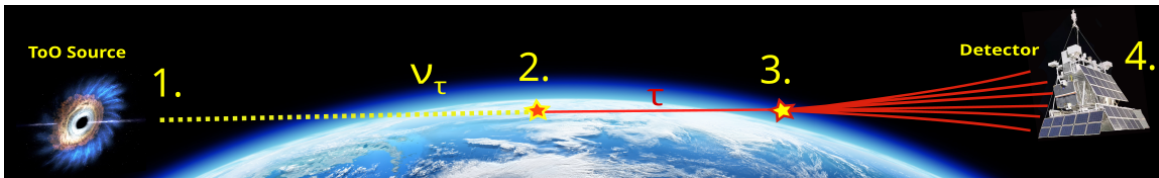


Figure 2.5 Illustration of the Earth skimming method used for neutrino detection 1. A neutrino source crosses the Earth's limb as viewed by the CT. 2. A neutrino from the source crosses through the Earth and interacts 3. A tau lepton is created in this interaction and propagates, leaving the Earth. 4. The tau-lepton decays in the atmosphere and produces an extensive air shower, which is observed by the CT. Fig. from ref. [31].

Neutrino emission due to transient or bursting/flaring extragalactic sources require follow-up observations to be performed within a couple of weeks (within one week for the strongest emission) after a neutrino signal is identified. EUSO-SPB2 is able to quickly respond to potential alerts of neutrino sources from pre-existing detectors to help improve correlation analysis. EUSO-SPB2 seeks to do this through its ToO program. The ToO program collects alerts from preexisting detectors, compiles a database and schedules follow-up observations for each night of operation as described in the following sections.

CHAPTER 3

THE ESUO-SPB2 TARGETS OF OPPORTUNITY

What follows is a brief summary of the motivation for the source types selected as ToO candidates for EUSO-SPB2.

3.1 Sources of Interest

The ToO sources of interest for EUSO-SPB2 include galactic and extra-galactic supernovae, binary neutron star mergers, neutron star-black hole mergers, nearby tidal disruption events, flaring blazars, gamma-ray bursts, and other transients (see Figure 3.1). It has long been theorized that sources such as these may produce VHE neutrinos [25]. Observations such as that of IceCube-170922A in which a neutrino of energy between 0.1-1 PeV was detected in association with a flaring blazar, have further motivated these searches [19].

The transients listed above may result in rapidly-spinning magnetars that can accelerate particles to ultra-high energies. These accelerated UHECRs may then produce TeV and above VHE neutrinos through interactions with the surrounding environment [32, 33]. Tidal disruption events (TDEs) accrete material and produce a flare of radiation that can last from months to years. Some TDEs result in powerful, relativistic jets which may act as proton and nuclei accelerators capable of reaching ultra-high energies that in turn produce VHE neutrinos through secondary collisions [34, 35]. Blazar flares and active galactic nuclei can produce ultra-high energy neutrinos through the interaction of accelerated cosmic rays with photon and baryon backgrounds [36, 37]. Supermassive binary black hole (BBH) mergers may also accelerate still-present material to ultra-high energies which would produce neutrinos through interactions with the surrounding environment, though the potential for these jets is still disputed [32, 38]. Short duration transients, such as gamma-ray bursts (GRBs), may also produce ultra high energy neutrinos [39, 40]. Due to their short duration and small radiation zone, their strong magnetic fields and radiation backgrounds may limit the maximum energies of transient neutrinos to the EeV range or below [41]. However, GRBs have promising implications for both VHE neutrino searches, potentially also in conjunction with gravitational wave detection, and their observations are still relatively new and without an identified upper energy limit.

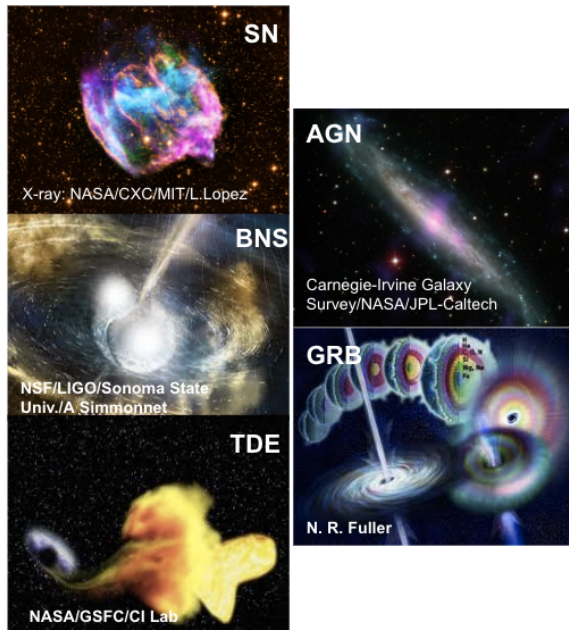


Figure 3.1 Artist representations of some of the types of sources of interest to the EUSO-SPB2 targets of opportunity program.

3.2 ToO Catalog

With the goal of optimizing the scientific reach of the ToO program within the operational parameters of the EUSO-SPB2 mission, a catalog of sources was developed from three alert systems broadcast from various detectors. The ToO catalog is populated through a combination of manual and automated processes that parse alerts from the General Coordinates Network (GCN), the Transient Name Server (TNS), and the Astronomer’s Telegram (ATel). These alerts are monitored and sorted based on their relation to potential neutrino sources of interest. GCN and TNS alerts are sorted by a python script, and ATel alerts are sorted by hand. The EUSO-SPB2 ToO catalog also includes a list of hand-selected steady sources (Table 3.1 and Table 3.2). For the EUSO-SPB2 observation period on May 14, 2023, the ToO catalog contained 102 sources (see Appendix B for the full list).

Each catalog (ToO) entry includes the reported observation time and observation coordinates of the alert. If the information is available via the respective alert system, the redshift and other characteristics are calculated and included in the catalog entry. Next, each source is assigned a priority value. These priority values are assigned based on the scheme presented in Section 3.3. From this information, the time and pointing direction for each ToO can then be calculated. ToO observations are scheduled for each nightly period of possible CT operation based on the values included in their catalog entries. More information on this scheduling process can be found in [42, 43].

Table 3.1 Part 1 of the complete list of steady sources included in the ToO source catalog for May 14, 2023. These sources are never removed from the catalog.

<i>Galactic Center</i>	<i>M 83</i>	<i>NGC 253</i>
-29d00m36s, 266d24m36s	-29d52m12s, 204d15m00s	-25d17m24s, 11d53m24s
<i>LMC</i>	<i>M 82</i>	<i>Cen A</i>
-69d45m36s, 80d53m24s	69d40m48s, 148d58m12s	-43d01m12s, 201d21m36s
<i>Old TA Hotspot</i>	<i>NGC 1068</i>	<i>Mrk 421</i>
40d30m00s, 144d00m00s	-0d00m04.68s, 40d40m12s	38d12m36s, 166d06m36s
<i>New TA Hotspot</i>	<i>Circinus</i>	<i>Mrk 501</i>
36d00m00s, 17d24m00s	-65d20m24s, 213d18m00s	39d45m36s, 253d28m12s
<i>IC 342</i>	<i>NGC 4945</i>	<i>3C 371</i>
68d06m00s, 56d42m00s	-49d28m12s, 196d21m36s	69d49m12s, 271d42m36s
<i>BL Lacertae</i>	<i>1ES 2344+514</i>	<i>H 1426+428</i>
42d16m48s, 330d40m48s	51d42m00s, 356d46m12s	42d40m12s, 217d08m24s
<i>1ES 1959+650</i>	<i>1ES 1440+122</i>	<i>PKS 2155-304</i>
65d09m00s, 300d00m00s	12d00m00s, 220d48m36s	-30d13m12s, 329d43m12s
<i>1ES 1218+304</i>	<i>1ES 1101-232</i>	<i>PKS 2005-489</i>
30d11m24s, 185d21m36s	-23d30m00s, 165d54m00s	-48d49m48s, 302d21m36s
<i>H 2356-309</i>	<i>PG 1553+113</i>	<i>Markarian 180</i>
-30d37m12s, 359d47m24s	11d11m24s, 238d56m24s	70d09m36s, 174d06m36s
<i>1ES 0229+200</i>	<i>PKS 0548-322</i>	<i>1ES 0347-121</i>
20d16m12s, 38d13m12s	-32d16m12s, 87d39m36s	-11d58m48s, 57d21m00s
<i>1ES 1011+496</i>	<i>RGB J0152+017</i>	<i>1ES 0806+524</i>
49d25m48s, 153d46m12s	1d46m48s, 28d08m24s	52d19m12s, 122d30m00s
<i>RGB J0710+591</i>	<i>PKS 1424+240</i>	<i>RBS 0413</i>
59d09m00s, 107d36m36s	23d47m24s, 216d45m00s	18d45m36s, 49d57m00s
<i>1ES 0414+009</i>	<i>PKS 0447-439</i>	<i>SHBL J001355.9-185406</i>
1d05m24s, 64d13m12s	-43d50m24s, 72d22m12s	-18d53m24s, 3d28m12s
<i>RX J0648.7+1516</i>	<i>B3 2247+381</i>	<i>HESS J1943+213</i>
15d16m12s, 102d11m24s	38d25m48s, 342d31m48s	21d18m00s, 295d58m48s
<i>1RXS J101015.9-311909</i>	<i>1ES 1312-423</i>	<i>1ES 1215+303</i>
-31d18m36s, 152d33m36s	-42d36m00s, 198d44m24s	30d06m00s, 184d27m00s
<i>1ES 1741+196</i>	<i>1ES 0033+595</i>	<i>1ES 1727+502</i>
19d33m00s, 266d00m00s	59d47m24s, 8d49m12s	50d13m12s, 262d04m48s
<i>KUV 00311-1938</i>	<i>PKS 0301-243</i>	<i>H 1722+119</i>
-19d21m00s, 8d24m00s	-24d07m48s, 45d51m00s	11d52m12s, 261d16m12s
<i>RBS 0723</i>	<i>RGB J2243+203</i>	<i>PKS 1440-389</i>
11d33m36s, 131d48m00s	20d19m12s, 340d58m12s	-39d08m24s, 221d00m00s
<i>1ES 2037+521</i>	<i>PGC 2402248</i>	<i>1ES 2322-409</i>
52d19m48s, 309d51m00s	51d54m00s, 113d21m36s	-40d39m36s, 351d12m00s
<i>TXS 0210+515</i>	<i>TXS 1515-273</i>	<i>1ES 0502+675</i>
51d45m00s, 33d34m12s	-27d31m48s, 229d31m12s	67d37m12s, 76d58m48s
<i>3C 279</i>	<i>PKS 1510-089</i>	<i>4C +21.35</i>
-5d47m24s, 194d03m00s	-9d06m36s, 228d13m12s	21d22m48s, 186d13m48s
<i>PKS 1441+25</i>	<i>PKS 0736+017</i>	<i>B2 1420+32</i>
25d01m48s, 220d59m24s	1d36m00s, 114d49m12s	32d23m24s, 215d37m48s

Table 3.2 Part 2 of the complete list of steady sources included in the ToO source catalog for May 14, 2023. These sources are never removed from the catalog.

<i>PKS 0346-27</i>	<i>M 87</i>	<i>NGC 1275</i>
-27d49m12s, 57d09m36s	12d24m00s, 187d42m00s	41d30m36s, 49d57m00s
<i>FRB 20190212A</i>	<i>FRB 20190208A</i>	<i>FRB 20190417A</i>
81d24m00s, 276d06m00s	47d00m00s, 283d30m00s	59d19m12s, 294d50m24s
<i>FRB 20180916B</i>	<i>FRB 20190520B</i>	<i>FRB 20201124A</i>
65d42m36s, 29d30m00s	-11d17m24s, 240d31m12s	26d03m36s, 77d00m36s
<i>FRB 20180301A</i>	<i>FRB 20180814A</i>	<i>FRB 20190303A</i>
4d33m36s, 93d10m48s	73d40m12s, 65d35m24s	48d07m12s, 207d59m24s
<i>Westerlund I</i>	<i>Westerlund II</i>	<i>SNR G106.3+02.7</i>
-45d51m00s, 251d46m12s	-57d45m36s, 155d59m24s	60d49m48s, 336d52m12s
<i>Crab Nebula</i>	<i>LHAASO J1825-1326</i>	<i>LHAASO J1839-0545</i>
22d03m00s, 83d33m00s	-13d27m00s, 276d27m00s	-5d45m00s, 279d57m00s
<i>LHAASO J1849-0003</i>	<i>LHAASO J1908+0621</i>	<i>LHAASO J1929+1745</i>
-0d03m00s, 282d21m00s	6d21m00s, 287d03m00s	17d45m00s, 292d15m00s
<i>LHAASO J2018+3651</i>	<i>LHAASO J2032+4102</i>	<i>LHAASO J2108+5157</i>
36d51m00s, 304d45m00s	41d03m00s, 308d03m00s	51d57m00s, 317d09m00s
<i>1EA 0647+250</i>	<i>RGB J0136+391</i>	<i>MS 1221.8+2452</i>
25d03m00s, 102d41m24s	39d06m00s, 24d08m24s	24d36m36s, 186d06m00s
<i>RX J1136.5+6737</i>	<i>1RXS J023832.6-311658</i>	<i>1RXS J081201.8+023735</i>
67d37m12s, 174d07m48s	-31d16m48s, 39d38m24s	2d37m48s, 123d00m36s
<i>MRC 0910-208</i>	<i>1RXS J195815.6-301119</i>	<i>RGB J2042+244</i>
-21d03m36s, 138d15m00s	-30d11m24s, 299d33m36s	24d27m00s, 310d31m12s
<i>3C 66A</i>	<i>W Comae</i>	<i>MAGIC J2001+435</i>
43d02m24s, 35d40m12s	28d13m48s, 185d22m48s	43d52m48s, 300d18m36s
<i>S5 0716+714</i>	<i>VER J0521+211</i>	<i>S2 0109+22</i>
71d20m24s, 110d28m12s	21d12m36s, 80d26m24s	22d44m24s, 18d01m12s
<i>S3 1227+25</i>	<i>B2 1811+31</i>	<i>PKS 0903-57</i>
25d18m00s, 187d33m36s	31d44m24s, 273d24m00s	-57d34m48s, 136d13m12s
<i>AP Librae</i>	<i>OT 081</i>	<i>S3 0218+35</i>
-24d22m12s, 229d25m12s	9d39m00s, 267d53m24s	35d56m24s, 35d16m12s
<i>TON 0599</i>	<i>3C 264</i>	<i>FRB 20181119A</i>
29d15m00s, 179d52m48s	19d36m36s, 176d16m12s	65d08m24s, 190d30m00s
<i>FRB 20121102A</i>	<i>FRB 20200120E</i>	<i>Cygnus Cocoon</i>
33d05m24s, 83d02m24s	68d49m48s, 149d29m24s	41d10m12s, 307d10m12s
<i>LHAASO J1843-0338</i>	<i>LHAASO J1956+2845</i>	<i>LHAASO J2226+6057</i>
-3d39m00s, 280d45m00s	28d45m00s, 299d03m00s	60d57m00s, 336d45m00s

3.3 ToO Prioritization

The mission source catalog is continuously running and gets updated in real-time to add selected new alerts and to remove outdated alerts. It typically contains more than 150 sources. On a given night, it is possible for more than 10 of these sources to rise and set around the Earth’s limb and be pointed at by the EUSO-SPB2 CT. Because observation time is limited each night to typically 5 hours or less, prioritization of these ToOs is required to ensure the most promising sources are viewed by the CT during the observation run. The process to develop the EUSO-SPB2 prioritization scheme considered existing HE-VHE neutrino source models, coincidence studies, the rate of occurrence for each ToO source type, and the age of the source. The final prioritization scheme (Table 3.3) is summarized below.

Table 3.3 The list of ToO sources of interest and their respective priority values as assigned for the EUSO-SPB2 mission.

<u>Source Type</u>	<u>EUSO-SPB2 Priority Tier</u>
Galactic supernovae	1
Binary neutron star and black hole-neutron star mergers	2
Nearby tidal disruption events	3
Flaring blazar or active galactic nuclei	4
Gamma-ray bursts	5
Supernovae outside of the galaxy	6
Other transients	7
Steady sources	8

Galactic Supernovae: Supernovae are widely considered to be the strongest and most frequent source of cosmic neutrinos. While extremely rare, galactic supernovae are expected to produce the highest rate of detectable neutrinos [32, 44]. These characteristics earn the top priority spot in the ToO prioritization scheme.

Binary neutron star and black hole-neutron star mergers: The expected neutrino production rate of these events is contested, though it is expected that not every merger would result in a stable enough environment to produce neutrinos. Because of the theoretical nature of these sources’ relationship to neutrino production, binary neutron star and black hole-neutron star mergers have been placed at a lower priority. However, because of the rare nature of these events as well as the promising LIGO-VIRGO reports of candidate electromagnetic counterparts, these events have thus been awarded the number two priority spot [32, 33].

Nearby tidal disruption events: TDEs may result in powerful, relativistic jets which may produce very-high and ultra-high energy neutrinos [34]. Long duration TDEs are especially promising. However, very few nearby TDEs have produced such jets. This conditional promise of VHE neutrinos in addition to

the rare nature of nearby jetting TDEs earns them the third priority spot [41].

Flaring blazar or active galactic nuclei: Neutrino detection has already coincided with blazar flare events, as evidenced by IceCube-170922A in association with a flaring blazar, TXS 0506+056. Similar success is expected with other types of active galactic nuclei. However, these events are likely to produce neutrinos at sub-PeV energies and are therefore given a lower priority [19, 36, 37].

Gamma-ray bursts: Gamma-ray bursts are a type of short-duration transient. With a similar promise of high energy neutrinos as the TDEs, this event type is placed at a much lower priority due to its short duration and small radiation zone which may limit the maximum energy of neutrinos to the EeV range or below - much higher than the PeV range of the CT neutrino energy threshold [41].

Supernovae outside of the galaxy: Like galactic supernovae, supernovae outside the galaxy are widely considered to be the strongest and most frequent source of cosmic neutrinos. Unlike galactic supernovae, these events are only expected to produce tens of detectable neutrinos. This, despite the higher rate of occurrence, places the extragalactic supernova low on the priority list [32, 44].

Other transients: Due to their high power, transient sources are expected to supply a significant number of detectable neutrinos. Because of the specific expectations of the sources listed above, they have been included in the ToO prioritization scheme in a specific order. While all other transients are expected to provide a promising opportunity to detect neutrinos, the lack of knowledge and specificity of this category places them low on the priority list [32, 41].

Steady sources: Steady sources are much less time-dependent in their observation opportunities. While, for example, short-duration transients may only yield promising results for less than 5 days. It is this reason that the list of steady sources included in the ToO catalog is prioritized last. Because of this, all other sources will be scheduled before the steady sources, with the steady sources only being scheduled if there is remaining observation time.

3.3.1 A Note on Gravitational Waves

Following the first detection of gravitational waves by the LIGO-VIRGO experiment in 2016 [45], researchers have begun to include the detection of gravitational waves in their physical alert mechanisms that signal the potential for incoming VHE neutrinos [46]. While the sources listed above present a fairly comprehensive list of known VHE neutrino astrophysical counterparts, in the the three years of IceCube data prior to the first reported TeV-range neutrino detection by the detector in 2013, there were 37 high-energy neutrino events at energies between 20 TeV and 1 PeV of cosmic origin observed by IceCube which have no astrophysical association [47]. Interestingly, two of the 100 TeV-range neutrinos were detected during the initial LIGO-VIRGO observation periods, during which time not all three gravitational

wave detectors were operational, bringing into question the possibility of joint sources of gravitational waves and high energy neutrinos [46].

Promising candidates for coincident detection of gravitational waves and neutrinos are the gamma-ray bursts as discussed above. The duration distribution of gamma-ray bursts shows a bi-modality which enables the distinction between short (< 2 sec) and long (> 2 sec) events [48]. Short gamma-ray bursts are believed to originate from coalescing binaries involving at least one neutron star, which the GW170817 detection has confirmed [49]. As LIGO-VIRGO and the newly-operational KAGRA was scheduled to begin their 4th observing run on May 24, 2023 [50], the ToO program with the EUSO-SPB2 mission hoped to include alerts from these gravitational wave detectors in the source catalog. Unfortunately the observing run ultimately began after the EUSO-SPB2 mission had ended, and this idea was never brought to fruition. Additionally, any long-duration flight examples that have been included in this thesis in Section 6 utilized data from balloon flights that also ended before any alerts from the O4 run were published.

CHAPTER 4
THE EUSO-SPB2 TOO FOLLOW-UP MECHANISMS

The EUSO-SPB2 ToO program relied on several components to ensure real-time efficient and effective usability (Figure 4.1).

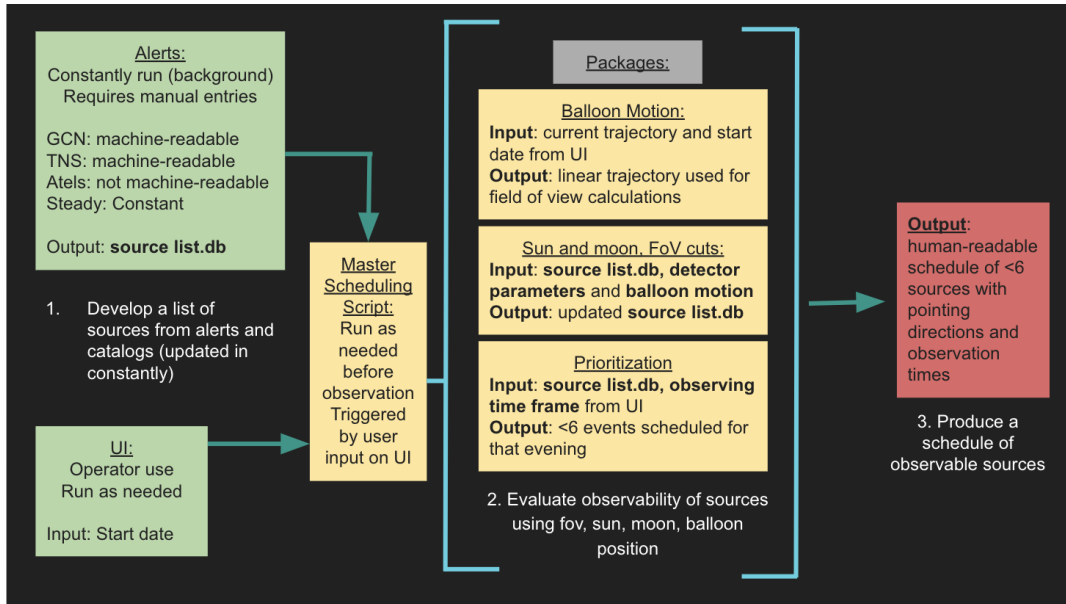


Figure 4.1 Step by step of the ToO scheduling software from receiving the alerts to scheduling ToOs for observation. Each step in this flowchart relates to a section in the software package created for that specific task.

4.1 ToO User Interface

The ToO software package comes with a user interface that was developed to enable cross-collaboration ease of use as well as external use. With the user interface, a researcher with limited knowledge of the underlying calculations and science is able to quickly and effectively search the database of neutrino detection alerts to develop a schedule of operations for a multi-messenger or follow-up detector.

The ToO user interface was developed in html, javascript and php, and can be hosted on a local or central server. When the user opens the site, they are first prompted to enter credentials, which are determined by the hosting organization. Once logged in, a local configuration file is generated for that particular user which the software package will refer to for file locations. The user is then able to enter the current or desired date into the scheduling system, and run the scheduler for that night of operation (Figure 4.2). The program will then produce a schedule of approximately 5 sources (depending on the moon

phase) for the given time period. This schedule includes the optimal pointing direction (dependent on the configuration of the detector which can be manually altered in the software package), the start and end time for observation, and an option to record whether the source has been observed at the end of the time period or not. Any user-entered information is recorded on the local computer in the downloaded package.

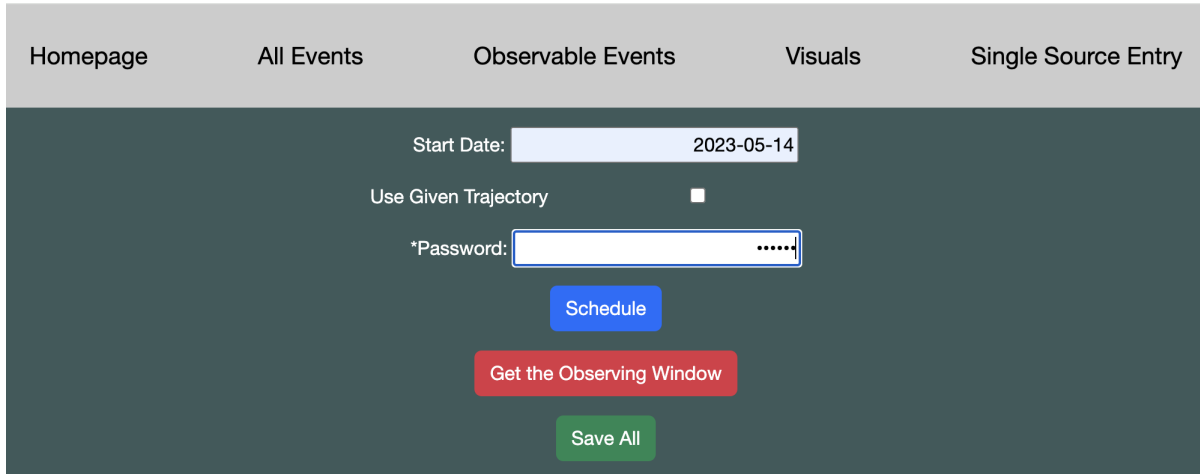


Figure 4.2 The user interface for the ToO scheduler. The user inputs the date of observation, a password, and selects "schedule". The ToO software package then takes the date of observation, calculates an observing window during which time the CT is able to detect neutrino emissions (based on moon phase and location) and schedules events from a database of alerts to maximize the possibility of detection by optimizing observation time

Other capabilities of the user interface include single-source entry, visualization packages, and database visualization. The single-source entry can be used for real-time alerts during operation. The database of sources is intended to run constantly in the background either on the local computer or on a central, accessible system, downloaded onto the local computer frequently. However, the updating of this database is not always as efficient as simply manually adding the details of an alert or source of interest. Thus, through the user interface, a user is able to enter the detection or location details of a source or alert of interest, immediately add it to the database and re-run the scheduler to see if the object is visible during the current observation period (Figure 4.3). The user has the option to assign the new entry top priority, lowest priority, or to follow the program's predetermined prioritization scheme. Top priority means the source will always be scheduled if it enters the field of view of the detector, lowest priority means it will only be scheduled if there is time remaining in the observation schedule and it enters the field of view of the detector, and the program's priority scheme is outlined in Section 3.3.

The screenshot shows a web interface with a navigation bar at the top containing five items: 'Homepage', 'All Events', 'Observable Events', 'Visuals', and 'Scheduler'. Below the navigation bar is a dark grey form area. The form contains the following elements from top to bottom:

- 'Source RA:' followed by a white text input field.
- 'Source Dec:' followed by a white text input field.
- 'Source Name:' followed by a white text input field.
- '*Observation Start:' followed by a white text input field.
- '*Observation End:' followed by a white text input field.
- '*Detector Altitude:' followed by a white text input field.
- A checkbox labeled '*Use Default'.
- 'Password:' followed by a white text input field.
- A blue button with white text that says 'Schedule This Source'.

Figure 4.3 The user interface for adding single sources to the ToO database and scheduler. If the user receives an alert during an observation run, they have the option to add this source to the database and see if it is able to be scheduled during the current observation period. This allows EUSO-SPB2 to quickly follow-up on real-time alerts

Visualization packages included in the user interface include detector visualization and source detection visualization. Detector visualization depends on the components of the detector that the program is configured for. In the case of EUSO-SPB2, this includes a map of the trajectory of the NASA-CSBF balloon carrying the detector, the field of view of the detector for the current period of observation, the overall field of view of the detector, and altitude information (for the purpose of determining the angle to the Earth’s limb from the detector). Source detection visualization includes a skymap of all possible sources to come into the field of view during the observation period, a skymap of the scheduled sources, and location/time plots of the scheduled sources which show when and where the scheduled sources enter the field of view of the detector during the current observation period. An example skymap for the night of May 14, 2023 is provided in Figure 4.4. By providing this information, an advanced user may be able to bring new insight into detector operations to make real-time decisions or alterations to the observation schedule in response to changing or unforeseen circumstances.

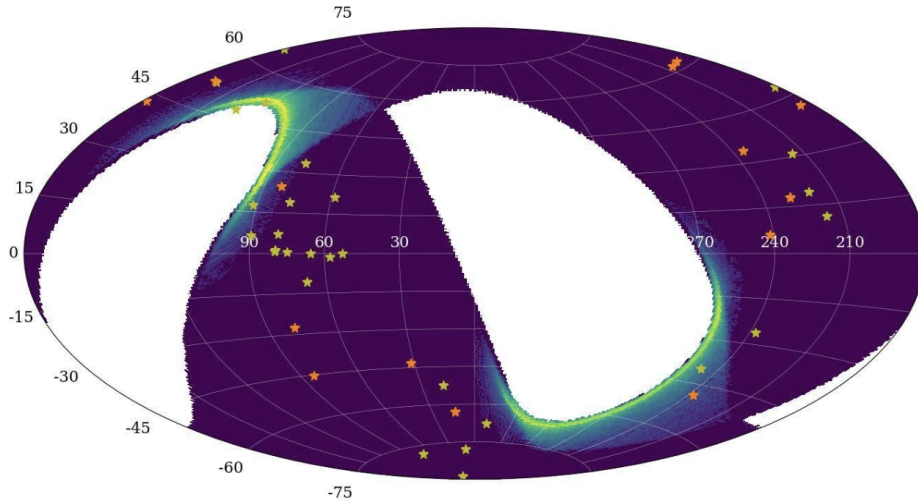


Figure 4.4 An example sky map visualization (in galactic coordinates) for all possible observable sources for the night of May 14, 2023. Transient sources are shown in orange and steady sources are shown in yellow. The deep blue to white gradient corresponds to the sensitivity of the EUSO-SPB2 CT. The white areas represent regions that are outside of the CT’s field of view, and the gradient blue to green areas near the white areas represent regions of lower sensitivity that sit on the edge of the CT field of view.

4.2 ToO Schedule Creation

A prioritization scheme is critical for the ToO scheduling process. The scheduling process, which is outlined in Figure 4.5, takes entries from the ToO catalog, compares their daily trajectories with the CT trajectory, and calculates the time and location of when the ToO will cross the detector’s field of view. After this is finished, there can be tens of sources that cross into the detector’s field of view during a nightly observation run. Because each of these runs may only be 4-5 hours at the most, with each ToO being visible anywhere from 20 minutes to 1 hour and 20 minutes, 4 or 5 sources at most may be scheduled (see Figure 4.6). The prioritization scheme is used to trim down the observable ToOs to fit the observation run schedule.

For a given observation period, if the number of observable sources is more than 5, the ToO software parses through the observable sources and chooses 4-5 based on priority values. This process involves 7 rounds of scheduling. Each round the software searches for a new priority value. If a transient source (the first 7 priority ratings) is observable with that priority value, it gets scheduled. If not, the program moves onto the next priority value. This continues until 4-5 sources are scheduled. If after 7 rounds there remains time in the observation period, the process starts again. The software will continue to fill the available time until each observable source has been checked. If there are not enough observable transient sources to fill the schedule, the program fills the schedule with observable steady sources (priority 8 sources).

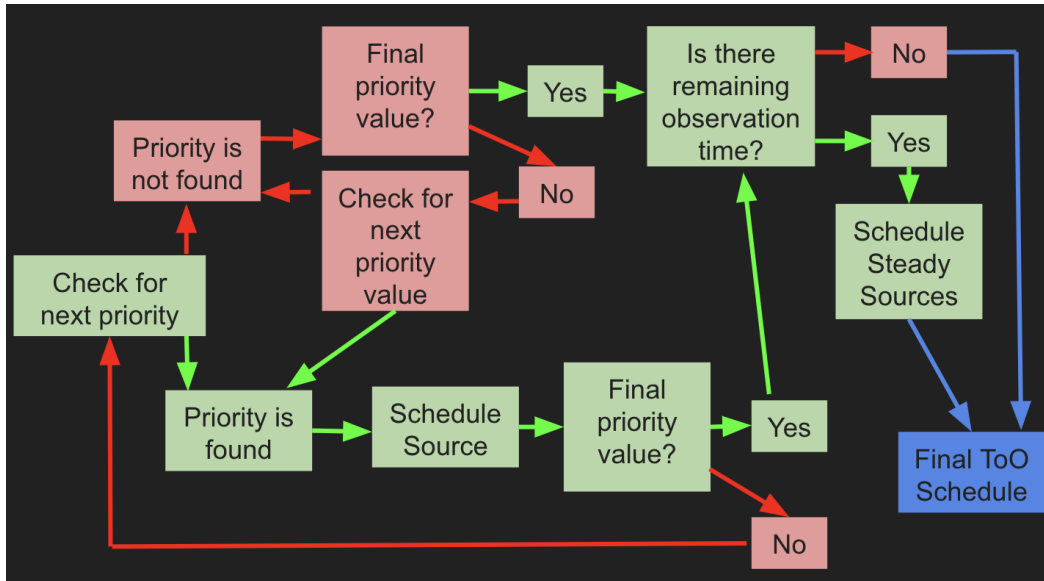


Figure 4.5 Flowchart of the ToO scheduling process. The scheduler goes through each priority value, only scheduling one source per priority until all values have been checked. Steady sources are scheduled to fill any remaining observation time.

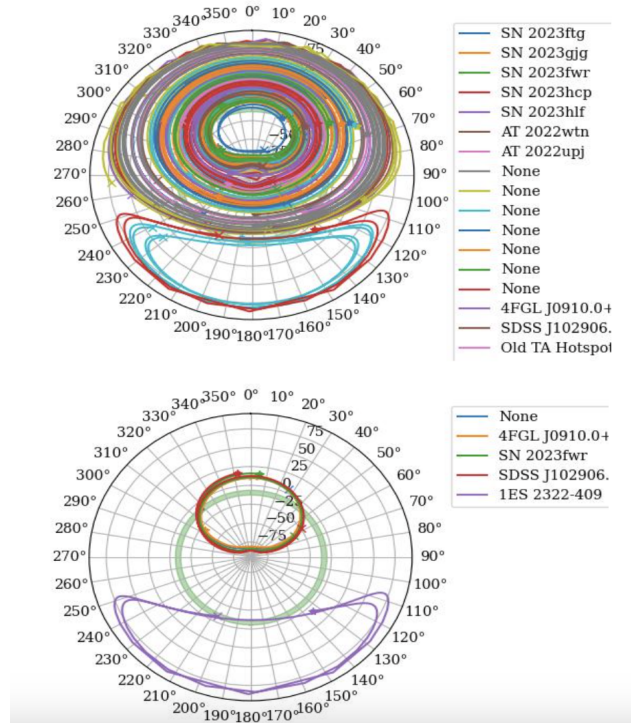


Figure 4.6 Top: An example of the trajectories of ToOs in the EUSO-SPB2 Cherenkov detector field of view before prioritization on May 14, 2023. There are approximately 70 ToOs that come into the field of view during this time - many more than can reasonably be observed during a single observation run. Bottom: the trajectories of ToOs in the EUSO-SPB2 Cherenkov telescope field of view after prioritization on May 14, 2023. The number of sources has been reduced to 5 for the average 5 hour observation window. The green circle on each of these plots represents the field of view, and the radius represents the altitude.

If there are multiple observable transient sources of a given priority value, the software checks a database of how much time the sources have already been observed. This database is updated after every observation run and records the observed sources with the amount of time (in minutes) of the ToO observation. Sources that have less recorded previous observation time in the database are prioritized over sources that have already been observed. An example schedule from May 14, 2023 is included in Table 4.1.

Table 4.1 Schedule produced by the software for May 14, 2023. For each source, we show the CT pointing, the move, start and end times in UTC. For the pointing we only indicate the azimuth (in degrees), as in the VHE neutrino observation mode the altitude is fixed to -9° .

<i>Source type, name</i>	<i>Pointing (az)</i>	<i>Move time</i>	<i>Start time</i>	<i>End time</i>
AGN, SDSS J102906.69+555625.2	47.19°	05:00	05:10	05:30
Steady FRB, FRB 20181119A	6.23°	05:30	05:40	06:10
SN II, SN 2023ftg	81.76°	06:10	06:20	06:50
AGN, 4FGL J0910.0+4257	315.96°	07:50	08:00	08:40
GRB, GRB230503A	187.66°	09:10	09:20	10:40

4.3 Shutter/Tilt System

The CT utilizes a tilt and rotation system to point the CT at scheduled ToOs. The CT's field of view is 6.4° in altitude and 12.8° in azimuth. The entire payload can be rotated 360° in azimuth and the CT can be tilted over a range of 10.3° (see Figure 4.7).

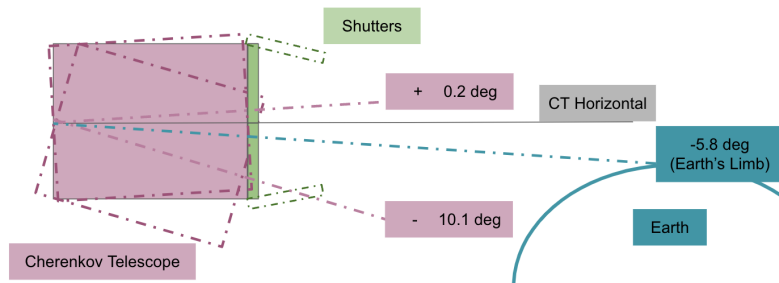


Figure 4.7 Field of view of the EUSO-SPB2 Cherenkov detector. The detector utilizes a tilt and rotation system to achieve a field of view of 6.4° in altitude and 12.8° in azimuth, and a rotational range of 360° in azimuth and a tilting range of 10.3° .

This system was comprised of a linear stage with a gear reducer moved by a stepper motor (the tilt motor), two temperature sensors, two shutters moved by two separate stepper motors (the shutter motors), two light sensors, and two inclinometers (tilt sensors) (see Figure 4.8). The entire system was controlled by a programmable logic computer which was housed in an insulated box on the gondola (see Figure 4.9 on page 24).

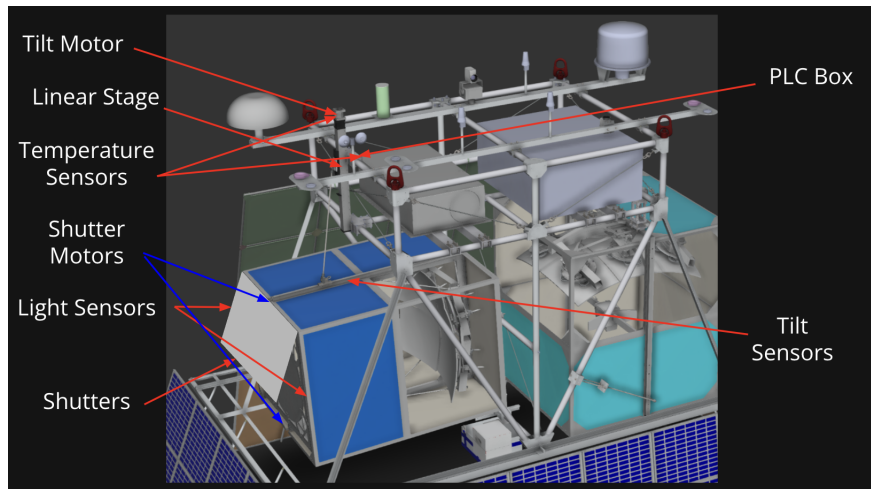


Figure 4.8 A rendering of the fully configured EUSO-SPB2 detector with the locations of the ST system components labeled in red and blue.

4.3.1 The PLC Box

The PLC box, shown in Figure 4.9, housed the brain of the S/T system. Composed of a programmable logic computer, three driver boards, an ethernet connection, a heater, and a power connection, the PLC box connected the tilt motors, limit switches, and shutter motors to the gondola control computer that relayed commands from the ground operator. The system’s software was programmed using Siemens’ SIMATIC STEP 7 Professional (TIA Portal) and was controlled via a ground-based computer (or ground-support equipment (GSE)) (more information on the user-operation can be found in Appendix A).

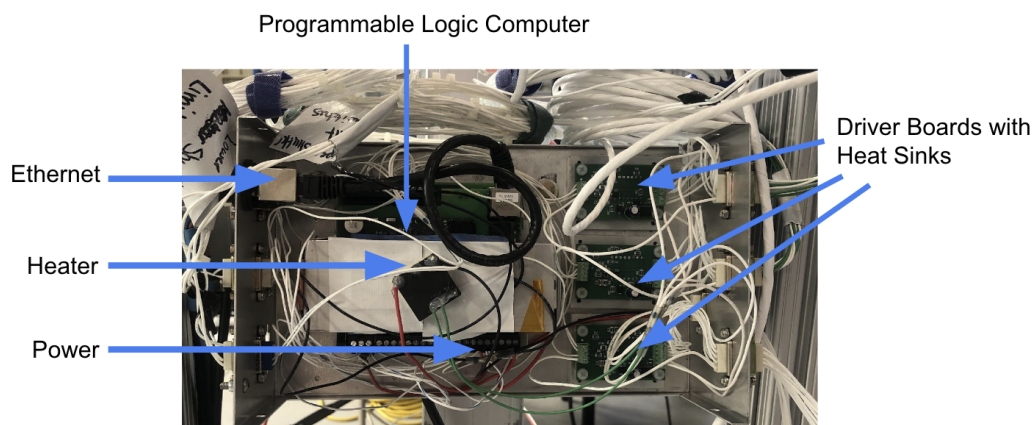


Figure 4.9 Internal view of the PLC Box that housed the communicative portion of the ST system, the Programmable Logic Computer (PLC). To run the PLC and connect its output to the various ST motors, the box also housed ethernet connections, a heater, power connections and three driver boards each with heat sinks attached

4.3.2 The Tilt System

The Tilt system, shown in Figure 4.10, composed of the linear stage, the tilt motor, a temperature sensor, and the inclinometers, was used to tilt the CT up and down a span of 10.3° (Figure 4.7). When the CT is centered directly on the Earth's limb, the angle measured is -5.8° relative to horizontal at the balloon. Therefore, the CT has an effective field of view of 4.3° below the limb to 6.0° above the limb.

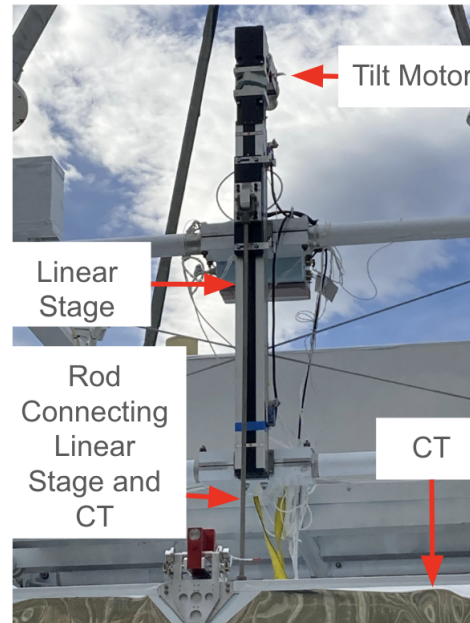


Figure 4.10 Assembled tilt mechanism. The tilt mechanism enables the CT to tilt from 7.3° below the limb to 8.3° above the limb, for a limb angle at 33 km of -5.8°

When connected to and controlled by the PLC system, the linear stage moves a number of steps which is recorded by the PLC program. The PLC program then converts this number of steps to degrees based on a calibrated formula and returns this information to the user via the GSE. The inclinometers also record the initial and final angle of inclination. Each inclinometer is voltage-mapped to 3 bytes (0-4095 decimal). One inclinometer is connected to the PLC box and is mapped -20 deg to 20 deg for 0-10 V. The second inclinometer is connected to the science stack and is mapped -10 deg to 10 deg for 0 - 5V. This means that, depending on the angle of inclination, the inclinometer produces a voltage of 0-5V or 0-10V. This voltage, for the inclinometer connected to the PLC box, is recorded by the PLC program, converted to a value between 0 and 4095, and reported to the user via the GSE using three bits in a status message. The voltage from the other inclinometer was converted to degrees by the CSBF science stack logging system.

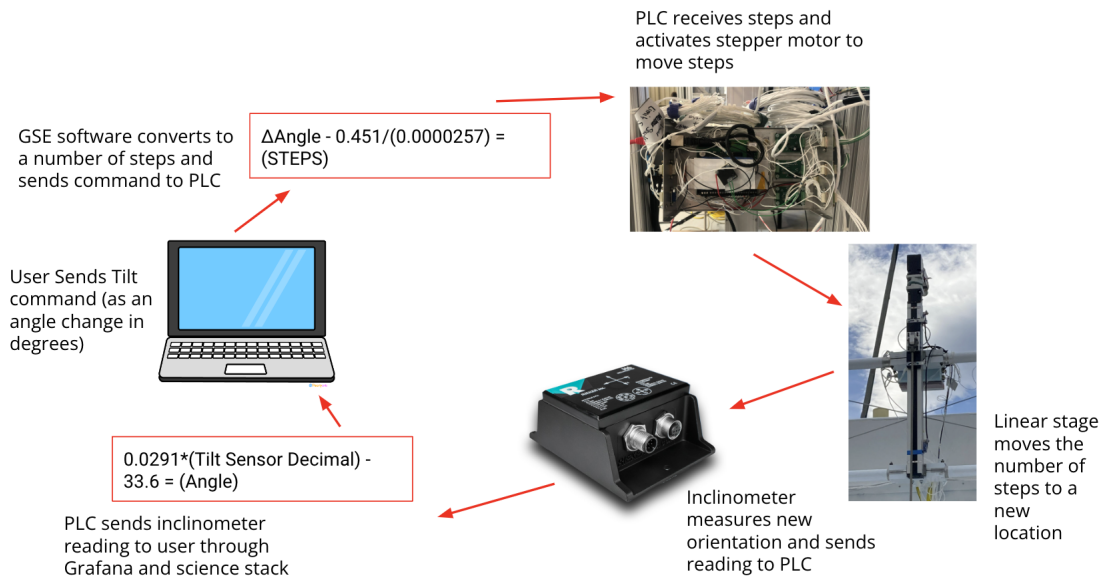


Figure 4.11 Flowchart of the tilt operation

To control the tilt of the CT, a user sends the desired angle change via a command from the GSE to the PLC box. The PLC program then converts this angle change to a number of steps for the stepper motor that moves the linear stage. The PLC sends a voltage pulse to the linear stage stepper motor depending on how many steps the stage needs to move. The uncertainty in the recorded position of the CT comes from this series of commands, conversions, and measurements as shown in Figure 4.11. The calibration of these measurements and conversions is outlined below.

4.3.3 Calibration and Testing of the Tilt System

This system was calibrated to an uncertainty of approximately 0.12 degrees. The inclinometers and linear stage were all tested and calibrated independently from one another before being tested and calibrated as a whole system. The inclinometers were calibrated using the setup in figure Figure 4.12. Specs for the Reiker inclinometers that were used can be found in Appendix A.

After this setup was configured, the tilt sensor was angled up and down in approximately one degree increments until a sweep of the inclinometer range was covered. The data shown here is recorded from the -20 deg to 20 deg inclinometer, from which the data was reported directly to the user over the ST interface. First, each angle was measured using a level, and that value was compared against the reported angle from the inclinometer (see Figure 4.13). Because the inclinometer reports angle as a voltage mapped to 3 bytes (4095 in decimal), the goal of this calibration was to determine a conversion between the reported bit value and the angle in degrees. The conversion equation was found to be, with an uncertainty of 0.1 degrees.

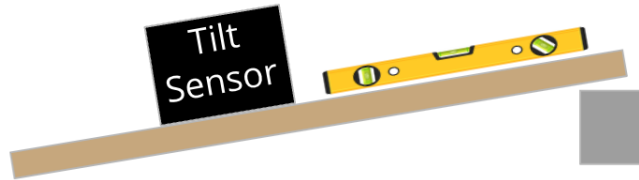


Figure 4.12 The setup for calibration of the inclinometers. The calibration process tilted the sensor at small angular intervals between -10° and 10° and between -20° and 20° for the science stack and GSE inclinometers respectively

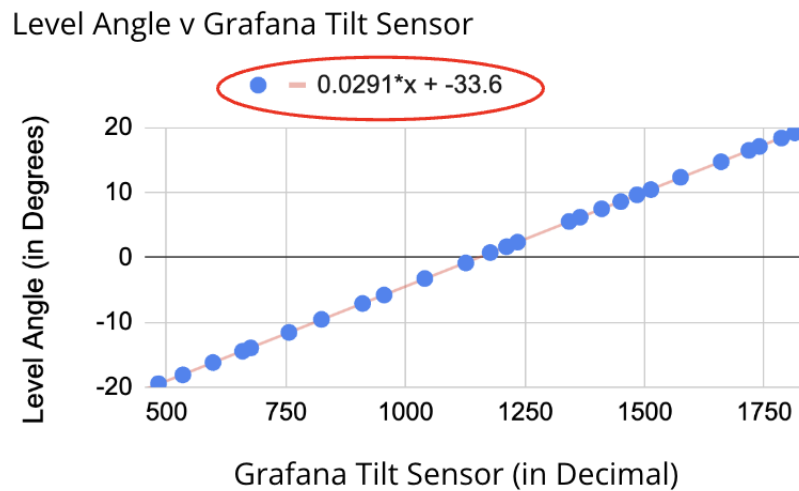


Figure 4.13 The resulting calibration curve for the GSE inclinometer. At each step, the angle in degrees from the level was recorded and plotted against the decimal representation reported by the PLC to the operator. A conversion equation was found to convert the reported decimal value back into an angle in degrees for ease of use. This equation is circled in red.

Once this conversion equation and its related uncertainty was determined, the next step was to ensure the process of moving the linear stage to a predetermined angle and then receiving the final angle from the inclinometer was understood. In order to do this, the linear stage and inclinometer were mounted in their final configuration (see Figure 4.10 and Figure 4.16). The user sent a number of steps to move the linear stage, and the inclinometer value before and after movement was recorded. The angle change was compared against the number of steps sent in order to determine a conversion between steps of the linear stage motor and the resulting angle change in order to enable the user to send a degree change rather than a number of steps (represented by the line of best fit in Figure 4.14 with the uncertainty found in Figure 4.15). This process was later changed so that the S/T interface program would take in the angle the user wanted to point, find the difference between this desired angle and the current angle reported by the inclinometer, convert it to a number of steps, then move the linear stage.

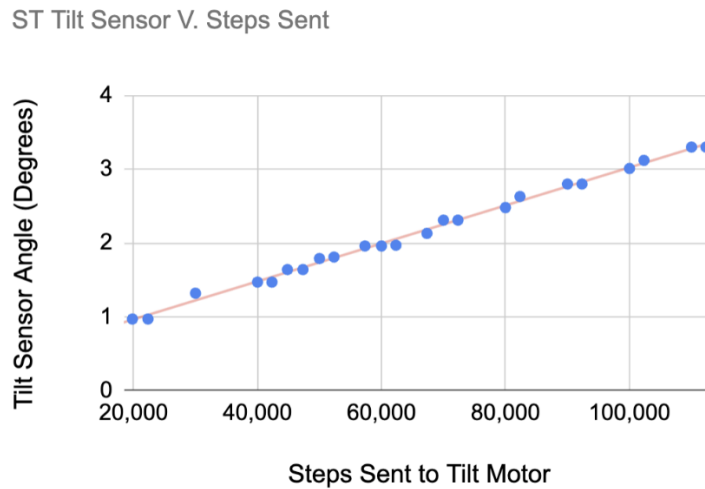


Figure 4.14 The calibration curve resulting from rigorous testing of the tilt mechanism. For this test, the operator sends a number of steps to move the linear stage to the PLC via the GSE. The linear stage moves and the resulting tilt angle in degrees is recorded from the GSE inclinometer. The resulting angle in degrees is plotted against the number of steps sent to the linear stage in order to determine a relationship between steps and a change in angle so that the operator may be able to send the desired angle that is then converted automatically into steps and sent to the PLC rather than sending number of steps each time for improved usability.

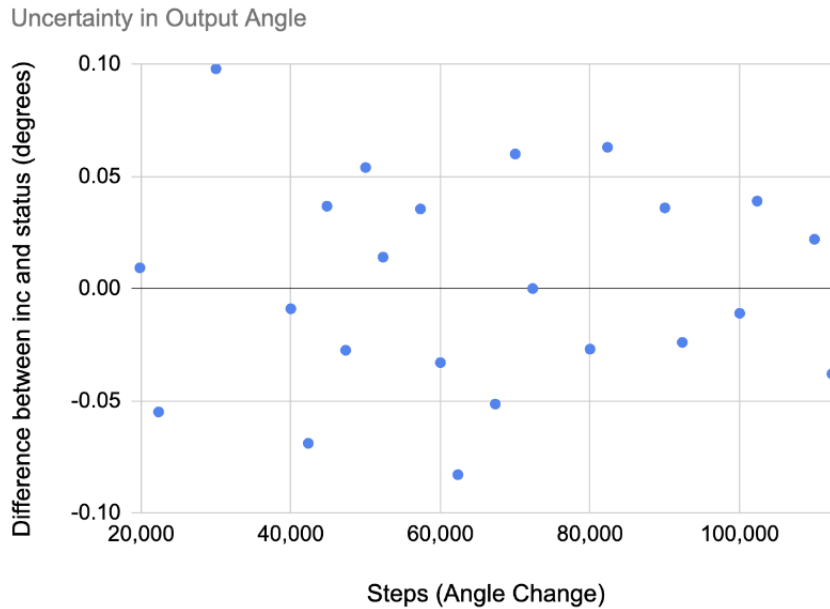


Figure 4.15 The uncertainty caused by the conversion equation between the voltage received by the PLC from the GSE inclinometer and the angle reported to the operator. The difference in the angle of the inclinometer and the angle reported to the operator through the PLC is plotted against the number of steps (angle change) that the linear stage is moved. Here it is seen that the uncertainty is larger for smaller angle changes (0.1 maximum) and smaller for larger angle changes (0.075 minimum).

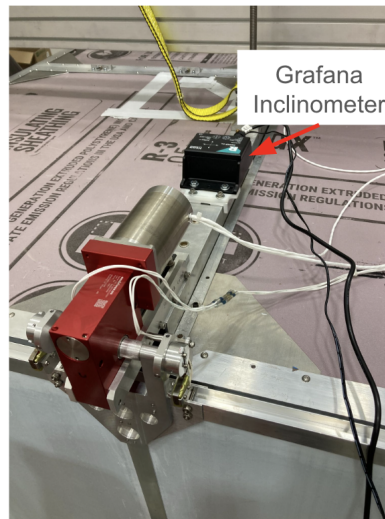


Figure 4.16 The inclinometer in its final location atop the CT frame, directly behind the top shutter mechanism. The inclinometer records the angle of the CT and outputs a voltage corresponding to that angle. The PLC receives this voltage and converts it back to an angle to report to the operator. The shutter actuator is also shown with a shutter motor mounted

4.3.4 The Shutter System

The Shutter system, composed of the two shutter mechanisms shown in Figure 4.17 and Figure 4.18, the upper and lower, two shutter motors, and light sensors, was used to protect the CT camera from external light sources, particularly the Sun during daylight hours. The shutters were controlled by means of the process in Figure 4.19 on page 30, in which the user sends a simple "Open" or "Close" command through the PLC box from the ground support computer, and the PLC sends a pulse to move the shutters. The shutter system also featured an automatic close operation if the user specified a specific amount of time for the shutters to be opened.

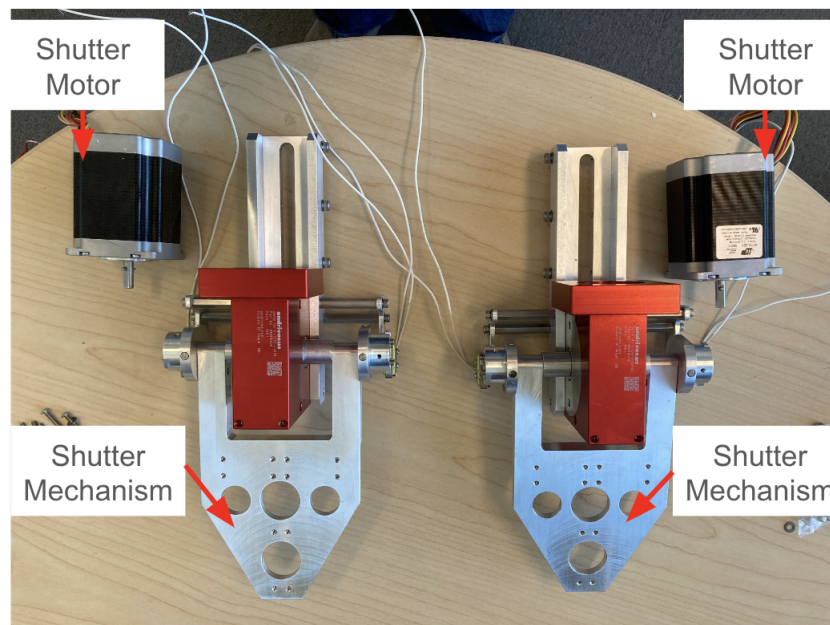


Figure 4.17 Top view of the shutter mechanisms, each powered by a stepper motor. The motors shown here are inexpensive versions used for early testing. The flight motors that were thermally tested and flown were provided by Empire Magnetics.

4.3.5 Calibration and Testing of the Shutter System

The calibration and testing process of the Shutter system was much more straightforward than that of the Tilt system. The shutter system is commanded by a simple Open/Close operation. To open the shutters, the command is sent to the PLC via the GSE, which then moves each shutter stepper motor a predetermined number of steps (top shutter first). To close the shutters, a similar process occurs but the motors are moved in the opposite direction until they trigger the respective limit switched, signaling to the PLC to stop sending power to the stepper motor (lower shutter first).

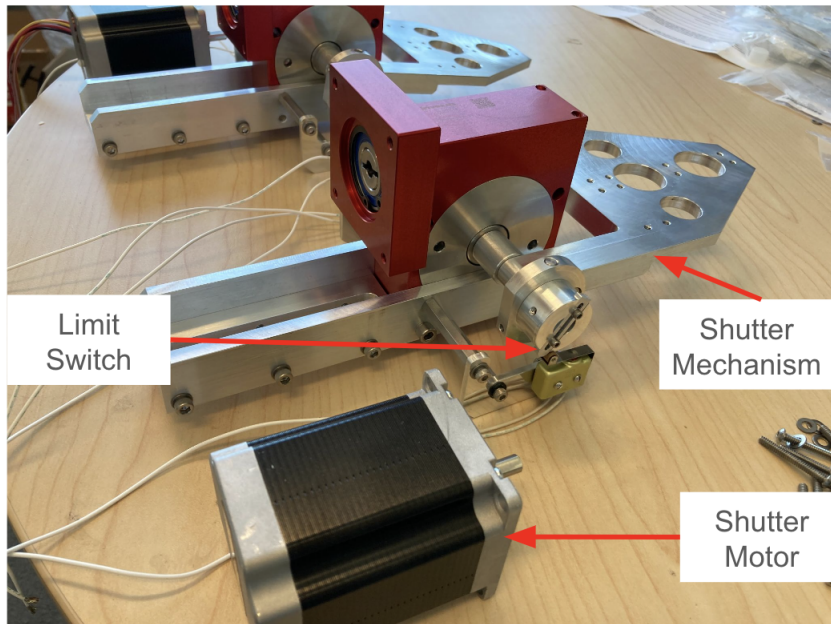


Figure 4.18 Side view of the shutter mechanisms, each powered by a stepper motor

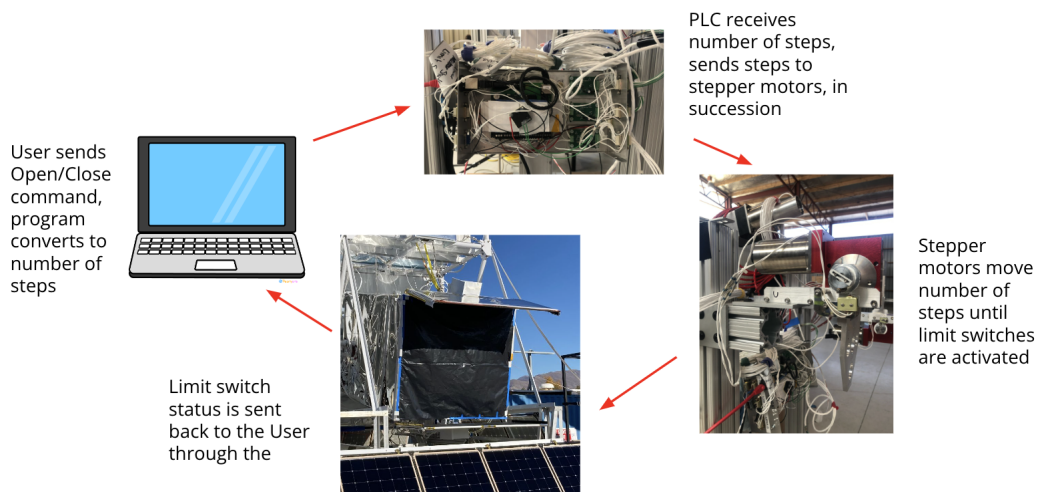


Figure 4.19 Flow chart of the shutter operation

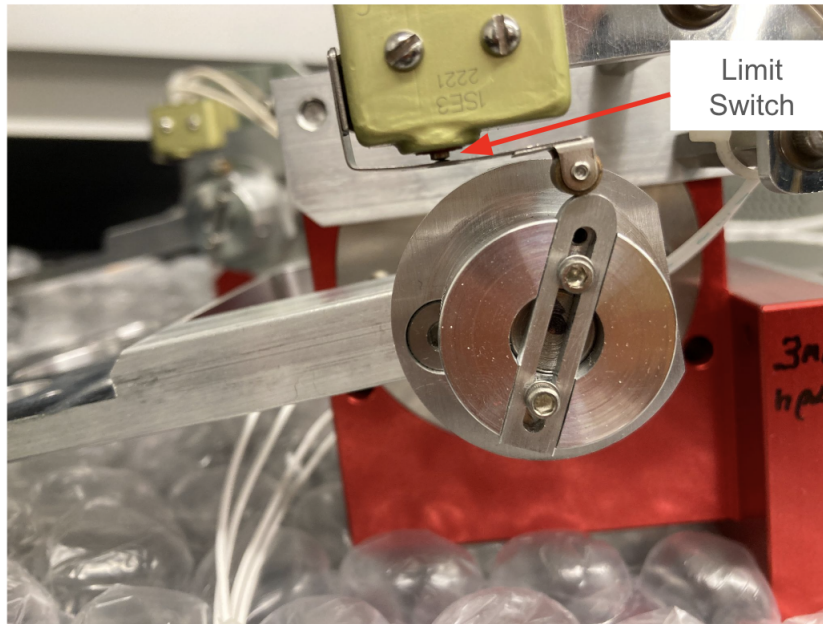


Figure 4.20 Limit switch used to stop each shutter from opening or closing too far. The limit switch may be set to a specific location for the opened and closed positions separately. When the either limit is reached, the PLC returns the "open" or "close" status to the operator via the GSE interface and stops the shutter motors.

The first round of testing included thermal testing down to -40C and up to 40C. This occurred at the NASA CSBF large thermal vacuum chamber testing facilities in Palestine, TX in November 2022. The shutter mechanisms were tested with weights attached (rather than the actual shutter doors) as there was not enough room in the chamber for the shutter doors and the linear tilt stage at the same time. The ST system performed adequately in these conditions showing no reproducible failures.

Based on the field of view of the CT, the operator moved each shutter a small amount until both were open enough with a few inches to spare beyond the field of view. The open limit switches on the upper and lower shutters, shown in Figure 4.20 were adjusted to stop the shutter motors at the position. The number of steps it took each shutter to reach the desired position was recorded and the Open command was reconfigured to require those steps. This was tested several times to ensure there was no slipping in the stepper motors. For final calibration and setting values, see Appendix A.

CHAPTER 5
PERFORMANCE RESULTS

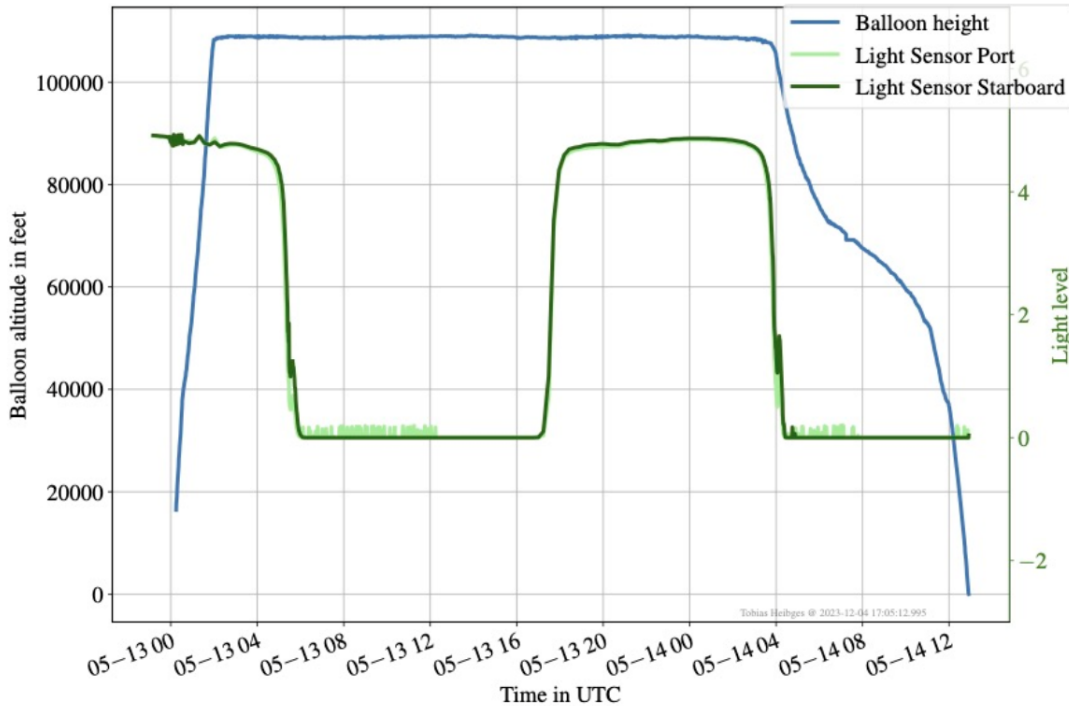


Figure 5.1 Plot of the altitude of the super pressure balloon carrying EUSO-SPB2 from 00:02 UTC May 13, 2023 to 12:54 UTC May 14, 2023. The balloon began losing altitude around 04:00 UTC on May 14, 2023 due to a leak in the balloon, and descended into the Pacific Ocean at 12:45 on May 14, 2023 UTC. This plot also displays the values of the light sensors aboard EUSO-SPB2. The possible observing periods of EUSO-SPB2 were between 08:00 UTC and 13:15 UTC on the first night and 04:45 UTC and 12:30 UTC on the second night, when these values were equal to zero. Plot provided by Tobias Heibges.

5.1 Shutter/Tilt Performance

The ST system performed adequately for the duration of the flight, whose altitude is plotted in Figure 5.1. Over both nights the shutters opened and closed on command, only timing out once on the first night when commanding was lost shortly. The tilt mechanism worked as expected, enabling the collection of 4 hours and 10 minutes of observation below the limb and 30 minutes above the limb the first night, and 6 hours and 25 minutes below the limb and 40 minutes above the limb on the second night.

There was a problem below about -36°C as measured at the tilt motor that was inside an insulated box. Starting around 08:30 UTC on the first night, the reported angle from the tilt sensor began to quickly drop over a 2-hour period. The inclinometers reported an unintentional decrease in tilt angle. Because no

commands were sent to the tilt motor, and there was no evidence that the motor had begun moving, this reported angle decrease was a result of the voltage output of the inclinometers dropping in the cold. This effect started at different times for the two inclinometers, confirming that the issue was with the inclinometers. With regards to commanding, at this temperature the commands sent to the tilt motor did not appear to move the linear stage and tilt the CT. A slight increase in the tilt motor temperature was observed after the command was sent that indicates the command was received. Outside of the observation period on the second day, the system warmed up. The tilting worked again until the temperature dropped below about -40C on the second night of observations. Based on the last previous known location of the tilt mechanism, an estimated pointing direction was extrapolated for the three times this error occurred over the two nights (see Figure 5.2). To do this, the angle was recorded after the system warmed up on the second day and this value was extrapolated backward to the value from the last known angle at the end of the first night.

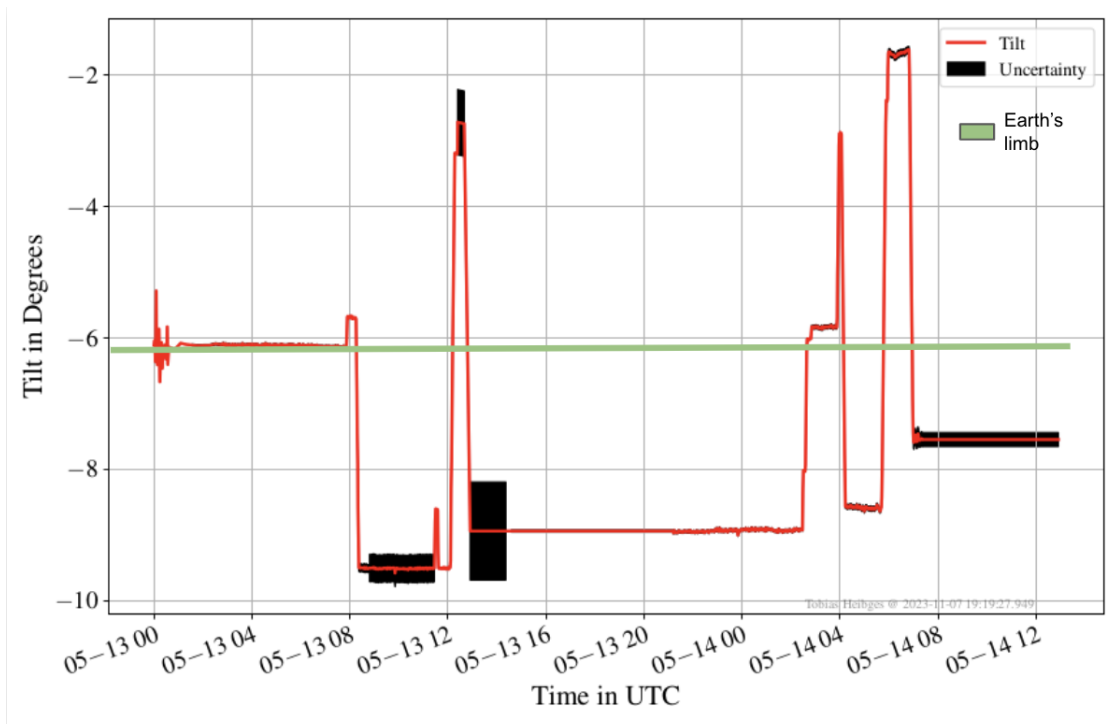


Figure 5.2 Plot of the uncertainty of the tilt mechanism over the duration of the EUSO-SPB2 flight. The tilt mechanism worked as expected resulting in 4 hours and 10 minutes of observation below the limb and 30 minutes above the limb the first night, and 6 hours and 25 minutes below the limb and 40 minutes above the limb on the second night. The limb here is located at -5.8 degrees assuming 110,000 FT elevation. The black regions indicate the estimated uncertainty in the tilt angle during these times. Plot provided by Tobias Heibges.

The shutters worked as intended during all temperatures encountered. The position of the shutters over the duration of the flight is show in Figure 5.3 and Figure 5.4. The ST system proved its utility above and below the limb - the CT recorded at least 10 promising cosmic ray events promising cosmic ray events when pointed above the limb.



Figure 5.3 The shutters were open for a total of 4h 40m during the first night of operation on May 13, 2023. Top: Upper shutter value; open = 5700 (steps), close = 0. Bottom: Lower shutter value; open = 5350 (steps), close = 0. The first open-close-open sequence at about 08:00 UTC was the first test of the system after launch. The shutters were opened initially for 15 minutes to test the auto-close function. After 15 minutes, the shutters closed and another command was sent to open the shutters for 30 minutes. Every 25 minutes another open command was sent to keep the shutters open for 30 more minutes. The close at about 12:00 UTC happened when the timeout after the last open command at 11:30 UTC. The next open-for-30-minutes command did not go through until after the shutters had closed. The shutters opened again after this command around 12:00 UTC and remained open using this same commanding process until the end of night 1 observations at 14:00 UTC.

5.2 ToO Performance

For EUSO-SPB2 ToO operations, the database of sources compiled from alerts during the several months prior to the flight - the source catalog - for both nights was 102 sources long, including 4 extragalactic supernovae, 1 galactic supernova, 3 TDEs, 5 GRBs, 2 AGNs, 2 flaring blazars, 2 unidentified sources and 93 steady sources. See Appendix B for the full list of sources in this catalog.



Figure 5.4 The shutters were open for a total of 7h 5m during the second night of operation on May 14, 2023. Top: Upper shutter value; open = 5700 (steps), close = 0. Bottom: Lower shutter value; open = 5350 (steps), close = 0.

Before the first night of operations on May 13th, 2023, the engineering period ToO operator utilized the user interface successfully create an efficient ToO pointing schedule for both nights to optimize the ToO viewing time. This process took the logged flight path provided by NASA CSBF with extrapolation and the observing window for each night to develop schedules that could have enabled the CT operators to strategically utilize the unexpectedly little time EUSO-SPB2 had. During the first night, the majority of the operation time was spent calibrating and verifying equipment operation.

During second night of observations, as the operators aimed to collect as much data as possible, it was extremely helpful to have a plan of observations. Instead of having to sort through the 20+ sources that may have come into the field of view, the CT operators had available the 5 prioritized targets for the mission - an active galactic nuclei and extragalactic supernova included (see Figure 5.5). With the limited operation time left, the CT operators decided to focus on measuring the night sky background and system performance below the limb. The CT was pointed below the limb to -7.6 degrees. Unable to point toward the sources on the schedule, the ToO operators were able to turn to the feature of the ToO software that determined all sources that passed through the field of view on a given night to see if any on that list could be see at the -7.5 degree angle. This feature saved the ToO operator precious time without having to sort through the 102 database sources, and at around 09:39 UTC, the researchers tried to rotate EUSO-SPB2 to +23 degrees azimuth to point toward FRB 20190417A.

Name	Type	Tier	Detection Start Time	Detection End Time	Move Time	Starting Location	Ending Location	Pointing Direction
FRB 20181119A	Steady FRB	8	2023-05-14T05:15:30.000	2023-05-14T06:35:30.000	2023-05-14T05:05:30.000	(-10.47 13.10)	(-12.29 344.41)	(-9.00 6.70)
SDSS J102906.69+555625.2	AGN	4	2023-05-15T02:55:30.000	2023-05-15T03:25:30.000	2023-05-15T02:45:30.000	(-10.38 47.54)	(-5.57 42.90)	(-9.00 46.01)
SN 2023fwr	SN Ic	6	2023-05-15T03:55:30.000	2023-05-15T04:35:30.000	2023-05-15T03:45:30.000	(-11.13 45.85)	(-4.98 39.67)	(-9.00 43.57)
4FGL J0910.0+4257	AGN	4	2023-05-15T04:55:30.000	2023-05-15T05:35:30.000	2023-05-15T04:45:30.000	(-6.27 321.40)	(-12.41 315.35)	(-9.00 319.10)
None		3	2023-05-15T06:55:30.000	2023-05-15T07:35:30.000	2023-05-15T06:45:30.000	(-6.08 320.94)	(-12.28 314.78)	(-9.00 318.60)

Figure 5.5 Out of the 102-source database, 5 sources were scheduled for night two of EUSO-SPB2 operations.

Unfortunately, as the night continued, and the altitude quickly dropped (see Figure 5.1 on page 32), operation of the rotator mechanism was lost because the thicker air at lower altitudes exerted too much drag on the rotation. After determining the stuck position to be +79 degrees in azimuth (North being 0 degrees), the team took another look at all of the possible sources that could cross the Earth's limb during that time (predetermined by the ToO program ran through the user interface) and tilted the CT to a location to hopefully encompass as many of those sources as possible (See Figure 5.6).

None	GRB	inf	2023-05-14T10: 15:30.000	2023-05-14T10: 55:30.000	(-6.12 222.30)	(-11.75 215.27)	(-9.00 219.71)
None	GRB	inf	2023-05-14T09: 15:30.000	2023-05-14T10: 55:30.000	(-6.16 194.63)	(-8.21 176.85)	(-9.00 188.23)
None		3	2023-05-14T10: 15:30.000	2023-05-14T10: 45:30.000	(-7.29 316.47)	(-12.19 312.87)	(-9.00 315.25)
NGC 253	Steady Seyfert	8	2023-05-14T10: 45:30.000	2023-05-14T10: 55:30.000	(-11.15 130.12)	(-9.37 128.39)	(-9.00 130.12)
Mrk 421	Steady Blazar	8	2023-05-14T10: 05:30.000	2023-05-14T10: 35:30.000	(-6.80 311.50)	(-12.10 307.79)	(-9.00 310.25)
SHBL J00135 5.9-185 406	Steady HBL	8	2023-05-14T10: 35:30.000	2023-05-14T10: 55:30.000	(-11.65 121.66)	(-7.69 118.33)	(-9.00 120.82)
1ES 2037+5 21	Steady HBL	8	2023-05-14T10: 45:30.000	2023-05-14T10: 55:30.000	(-10.94 33.22)	(-9.73 32.10)	(-9.00 33.22)
FRB 201904 17A	Steady FRB	8	2023-05-14T10: 25:30.000	2023-05-14T10: 55:30.000	(-11.86 24.29)	(-9.29 21.05)	(-9.00 23.23)

Figure 5.6 There were 8 sources that were not scheduled due to repeating priority values. These sources still may have passed through the EUSO-SPB2 field of view (if the detector had been pointing in the right direction).

A post-flight study of the logged data was conducted to determine the likelihood that a ToO was caught in the field of view, and found a few points of concern. First off, when rotator capabilities were lost, the balloon was falling quickly and turning as it did so. It is likely that some ToO sources crossed into the field of view through accidental coincidence while the CT looked below the limb. However, the rate of rotation was so quick that the ToO sources crossed the field of view in less than a minute. While this is not enough data to verify neutrino detection, the high-stake environment was a productive test for the ToO scheduling process and further improvements are currently being made in preparation to apply the process to a future flight.

CHAPTER 6
LONG DURATION FLIGHT STUDY

To explore the capabilities of the ToO program, the source cataloging and ToO scheduling processes were applied to the 39 day SuperBIT trajectory (Figure 6.1). SuperBIT circumnavigated the Antarctic circle 5 times. A study was executed using this flight path to determine the potential for viewing many more sources of interest as well as viewing the same source multiple times.

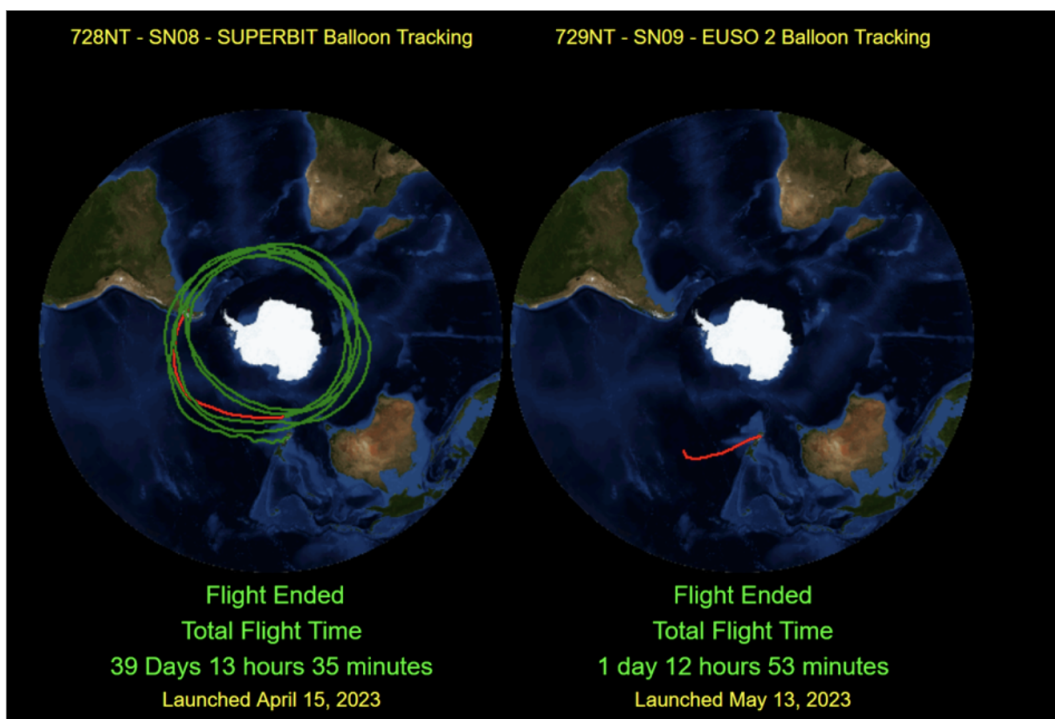


Figure 6.1 After final, rigorous testing on the ground in Wanaka, NZ, EUSO-SPB2 was launched on May 13, 2023. The flight lasted 1 day 12 hours and 53 minutes, and was terminated due to a leak in the balloon. In order to further test the ToO software, a simulation was run on the SuperBIT trajectory.

The study was run using an improved version (same scheduling/prioritization process, cleaner functions, more rigorously tested, etc.) of the ToO scheduling software that was developed for the EUSO-SPB2 mission. A CSV file of SuperBIT's flight trajectory was read in, and using those coordinates a ToO schedule was developed for each day of the flight.

This study found that an average of 2-3 sources were scheduled each night, with 8 nights scheduling no sources, 6 nights scheduling 5 sources, and the most common schedule included 4 sources (12 nights) as shown in Figure 6.2. There were 8 nights that scheduled no sources. April 22 is an anomaly that is

currently being looked into as it may be a result of a step being skipped in the scheduling process. May 4th to May 6th are expected to produce no observable sources as there was a full moon on May 5th so it was too bright for any observations. However, the extended effects into May 10th are unexpected and also currently being analyzed.

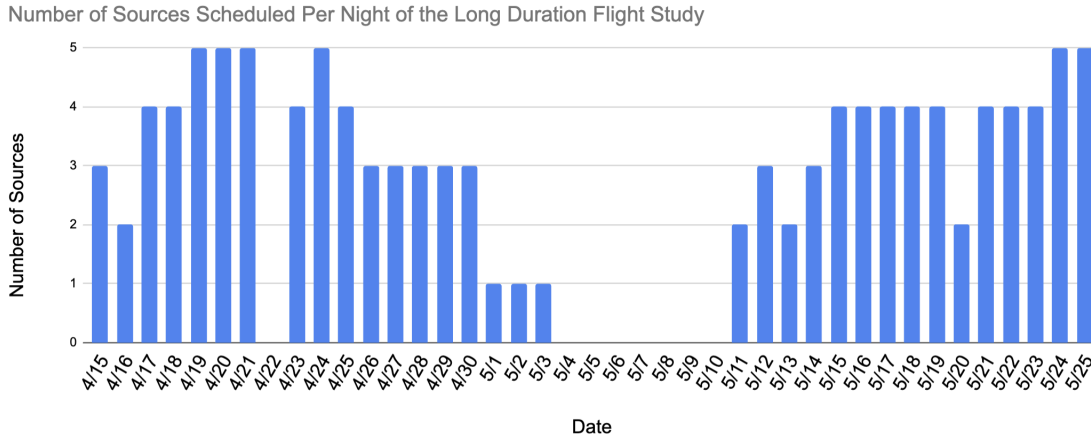


Figure 6.2 Over the span of 39 days, an average of 2-3 sources were scheduled each night.

Fourteen unique sources were scheduled over the 39 nights. Out of these sources there were 2 TDEs: AT 2022upj and AT 2023clx; 2 AGNs: SDSS J152205.41+393441.3 and SDSS J102906.69+555625.2; 2 Blazars: MG2 J144640+3110 and SDSS J102906.69+555625.2; 4 extragalactic supernovae: SN 2024btj, SN 2024bqr, SN 2024chx, and SN 2024byg; 1 FSRQ: PKS 2054-377; and 3 steady sources: The Old TA Hotspot, The New TA Hotspot, and the Galactic Center. This source ratio is shown in Figure 6.3. The frequency of these sources being scheduled is shown in Figure 6.4. The most frequently scheduled sources were AT 2023clx and MG2 J144640+3110, being scheduled on a total of 22 out of the 39 nights. The least frequently scheduled sources were the Galactic Center, PKS 0402-362, and SDSS J102906.69+555625.2 which were each only scheduled once out of the 39 days.

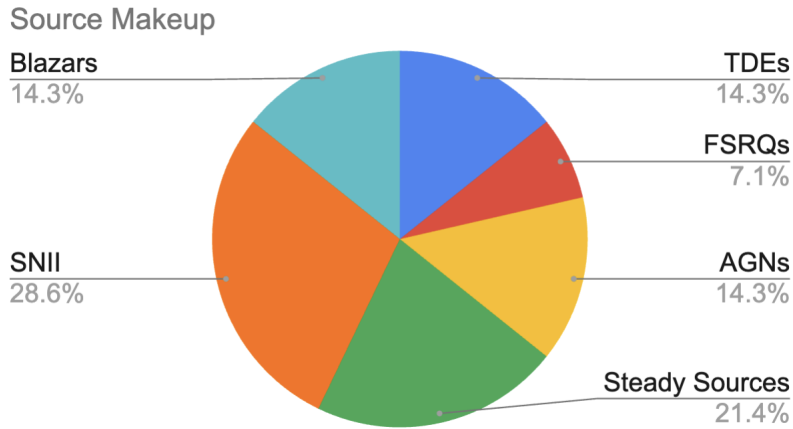


Figure 6.3 There was a total of 14 unique sources that showed up over the 39 nights. Out of these sources there were 2 TDEs, 2 AGNs, 2 Blazars, 4 extragalactic supernovae, 1 FSRQ, and 3 steady sources

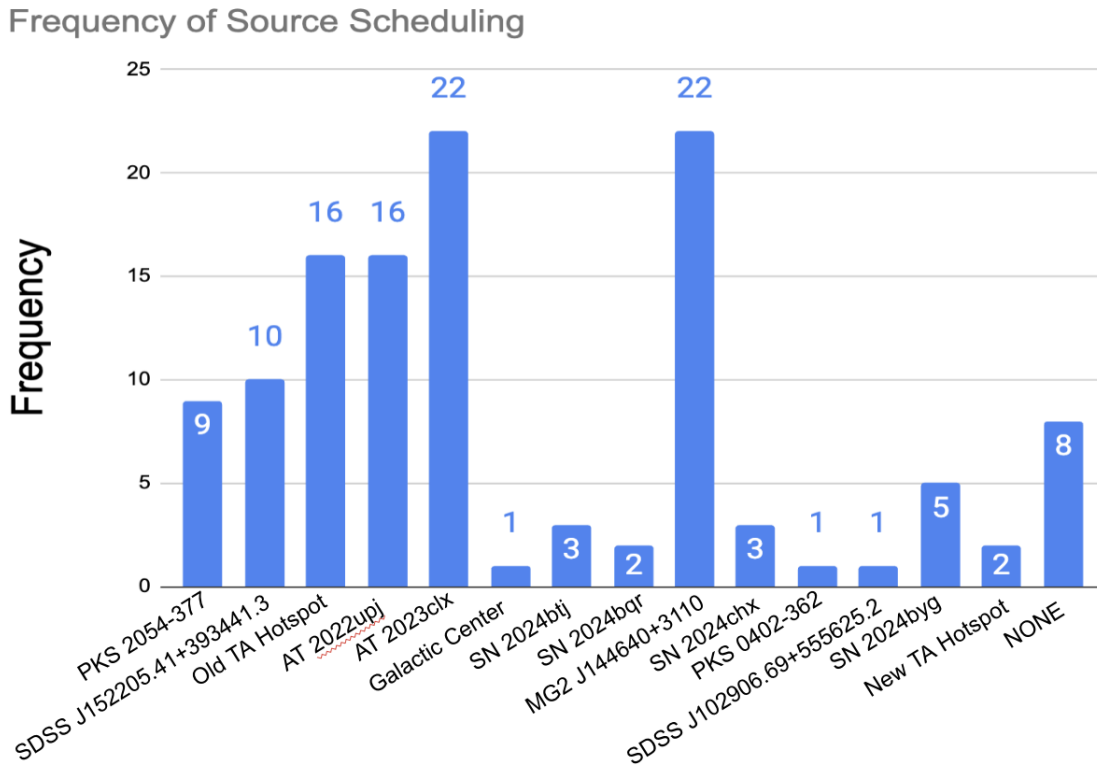


Figure 6.4 The most frequently scheduled sources were AT 2023clx and MG2 J144640+3110, being scheduled on a total of 22 out of the 39 nights. The least frequently scheduled sources were the Galactic Center, PKS 0402-362, and SDSS J102906.69+555625.2 which were each only scheduled once out of the 39 days

This study is currently in progress. As can be seen by the inclusion of SN 2024btj, SN 2024bqr, SN 2024chx, and SN 2024byg, the database of sources used for this study was created in early 2024 - not before the dates this flight study covers in 2023.

Work is currently ongoing to sort through the archives of source alerts from February 1, 2023 to May 25, 2023 in order to create a more accurate database from which to complete this study. All alerts from the GCN server during this time period have been parsed by hand and are being sorted through to create a database that may then be used to produce more accurate schedules for the long-duration flight study. Through this process, the ToO team has been able to get a more accurate understanding of how many alerts to expect in a given time period. These preliminary alert numbers are listed with their respective observatories in Table 6.1.

Table 6.1 The number of alerts the GCN received for each GCN-registered observatory from February 1, 2023 to May 25, 2023. Each operational observatory listed on the GCN server is included here for completeness, though the EUSO-SPB2 ToO program is only interested in alerts related to the sources of interest from Chapter 3.

<i>Observatory</i>	<i>Number of alerts from February 1, 2023 to May 25, 2023</i>
IceCube	19
LIGO/VIRGO/KAGRA	38
HAWC	3
IceCube-HAWC	4
IceCube Cascades	4
Calet	84
MAXI	19
Fermi GRBs	997
Fermi LAT	4
Swift GRBs	698
Fermi GBM Sub-Threshold	80
Integral GRBs	60
Integral SPI-ACS	29
Super-K	4 test notices
IceCube-HAWC Coincidences	4
AGILE MCAL	4

CHAPTER 7

CONCLUSION

Although the lifetime of EUSO-SPB2 was not as lengthy as anticipated, there are exciting takeaways from the EUSO-SPB2 mission. EUSO-SPB2 was the first time a Cherenkov telescope has flown on a balloon. It was the first time that cosmic rays EASs were detected from a balloon using the Cherenkov technique. And it was the first time a program has attempted to point a Cherenkov telescope at potential ToOs in response to real-time alerts to try to catch neutrinos.

These first-time opportunities motivated the development of a software package to parse three established databases of ToO alerts, prioritize these ToOs, and schedule the sources for observation. Unfortunately the loss of the payload after just 37 hours did not leave enough time to test this method thoroughly. Across the two nights of observation, there was not enough time allotted to point the CT at a ToO source. Nonetheless, the ToO program was ready to go, and able to be operated through a friendly user interface.

Since then, the software package has been back-tested using a different trajectory. As seen in the long-duration flight study, the ToO program produced consistent schedules that provided observation time over multiple nights of the same source, while including a good rotation between 14 unique sources.

The reliability of the physical follow-up mechanism, the ST system, further proved the feasibility of this ToO mission. By creating a system that could re-point across its tilt range in less than 30 minutes, and tilt a degree in less than 5 minutes, the observation time for each scheduled source was able to be maximized for an average of 40 minutes per source. The working shutter system ensured the detector was protected throughout the flight, and the reliable communication system ensured that the user knew what direction the CT was pointing at all times. The user-friendly and efficient ST system was effective at supporting the ToO mission at temperatures above -36C , enabling the CT to observe 4 hours and 10 minutes below the limb and 30 minutes above the limb the first night, and 6 hours and 25 minutes below the limb and 40 minutes above the limb on the second night of the EUSO-SPB2 flight.

Together the ST system and the ToO software are able to work together to provide a reliable, user-friendly, and efficient method of astrophysical neutrino detection follow-up. As ground-based detectors improve their sensitivity, follow-up mechanisms like that of EUSO-SPB2's ToO program are increasingly vital to the corresponding coincident studies and, specifically, critical to the science case for the next balloon mission (POEMMA Balloon Radio) planned for launch in 2027.

REFERENCES

- [1] Johannes Eser, Angela V. Olinto, and Lawrence Wiencke. Science and mission status of EUSO-SPB2. PoS, ICRC2021:404, 2021. doi: 10.22323/1.395.0404.
- [2] A. V. Olinto et al. The POEMMA (Probe of Extreme Multi-Messenger Astrophysics) Observatory. The Astrophysical Journal, 2020. doi: 10.1088/1475-7516/2021/06/007.
- [3] J. Eser et al. Overview and First Results of EUSO-SPB2. PoS, ICRC2023:0397, 2023. doi: 10.22323/1.444.0397.
- [4] E. Gazda et al. The EUSO-SPB2 Cherenkov Telescope - performance and preliminary results. PoS, ICRC2023:1029, 2023. doi: 10.22323/1.444.1029.
- [5] Xun-Jie Xu, Zhe Wang, and Shaomin Chen. Solar neutrino physics. Progress in Particle and Nuclear Physics, 131:104043, July 2023. ISSN 0146-6410. doi: 10.1016/j.pnpnp.2023.104043. URL <http://dx.doi.org/10.1016/j.pnpnp.2023.104043>.
- [6] P. Anselmann et al. Solar neutrinos observed by gallex at gran sasso. Physics Letters B, 285(4): 376–389, 1992. ISSN 0370-2693. doi: [https://doi.org/10.1016/0370-2693\(92\)91521-A](https://doi.org/10.1016/0370-2693(92)91521-A). URL <https://www.sciencedirect.com/science/article/pii/037026939291521A>.
- [7] Veretenkin Abdurashitov et al. Solar neutrino flux measurements by the soviet-american gallium experiment (sage) for half the 22-year solar cycle. Journal of Experimental and Theoretical Physics, 95:104043, August 2002. doi: 10.1134/1.1506424. URL <https://doi.org/10.1134/1.1506424>.
- [8] K. S. Hirata et al. Observation of ^8B solar neutrinos in the kamiokande-ii detector. Phys. Rev. Lett., 63:16–19, Jul 1989. doi: 10.1103/PhysRevLett.63.16. URL <https://link.aps.org/doi/10.1103/PhysRevLett.63.16>.
- [9] Y. Fukuda et al. Measurements of the solar neutrino flux from super-kamiokande’s first 300 days. Phys. Rev. Lett., 81:1158–1162, Aug 1998. doi: 10.1103/PhysRevLett.81.1158. URL <https://link.aps.org/doi/10.1103/PhysRevLett.81.1158>.
- [10] Q. R. Ahmad et al. Direct evidence for neutrino flavor transformation from neutral-current interactions in the sudbury neutrino observatory. Phys. Rev. Lett., 89:011301, Jun 2002. doi: 10.1103/PhysRevLett.89.011301. URL <https://link.aps.org/doi/10.1103/PhysRevLett.89.011301>.
- [11] Ningqiang Song, Shirley Weishi Li, Carlos A. Argüelles, Mauricio Bustamante, and Aaron C. Vincent. The future of high-energy astrophysical neutrino flavor measurements. Journal of Cosmology and Astroparticle Physics, 2021(04):054, April 2021. ISSN 1475-7516. doi: 10.1088/1475-7516/2021/04/054. URL <http://dx.doi.org/10.1088/1475-7516/2021/04/054>.
- [12] Aya Ishihara and for the IceCube Collaboration. Extremely high energy neutrinos in six years of icecube data. Journal of Physics: Conference Series, 718(6):062027, may 2016. doi: 10.1088/1742-6596/718/6/062027. URL <https://dx.doi.org/10.1088/1742-6596/718/6/062027>.

- [13] Naoko Kurahashi, Kohta Murase, and Marcos Santander. High-energy extragalactic neutrino astrophysics. Annual Review of Nuclear and Particle Science, 72(1):365–387, September 2022. ISSN 1545-4134. doi: 10.1146/annurev-nucl-011122-061547. URL <http://dx.doi.org/10.1146/annurev-nucl-011122-061547>.
- [14] C. L. Cowan, F. Reines, F. B. Harrison, H. W. Kruse, and A. D. McGuire. Detection of the free neutrino: a confirmation. Science, 124(3212):103–104, 1956. doi: 10.1126/science.124.3212.103. URL <https://www.science.org/doi/abs/10.1126/science.124.3212.103>.
- [15] Raymond Davis, Don S. Harmer, and Kenneth C. Hoffman. Search for neutrinos from the sun. Phys. Rev. Lett., 20:1205–1209, May 1968. doi: 10.1103/PhysRevLett.20.1205. URL <https://link.aps.org/doi/10.1103/PhysRevLett.20.1205>.
- [16] W. David Arnett, John N. Bahcall, Robert P. Kirshner, and Stanford E. Woosley. Supernova 1987a. Annual Review of Astronomy and Astrophysics, 27(Volume 27, 1989):629–700, 1989. ISSN 1545-4282. doi: <https://doi.org/10.1146/annurev.aa.27.090189.003213>. URL <https://www.annualreviews.org/content/journals/10.1146/annurev.aa.27.090189.003213>.
- [17] Christian Spiering. Towards high-energy neutrino astronomy: A historical review. The European Physical Journal H, 37(3):515–565, July 2012. ISSN 2102-6467. doi: 10.1140/epjh/e2012-30014-2. URL <http://dx.doi.org/10.1140/epjh/e2012-30014-2>.
- [18] M. G. K. Menon, S. Naranan, V. S. Narasimham, K. Hinotani, N. Ito, S. Miyake, R. Craig, D. R. Creed, J. L. Osborne, and A. W. Wolfendale. V. studies of cosmic ray neutrino interactions in the kolar gold field experiment. Proceedings of the Royal Society of London. Series A, Mathematical and Physical Sciences, 301(1465):137–157, 1967. ISSN 00804630. URL <http://www.jstor.org/stable/2415936>.
- [19] Multimessenger observations of a flaring blazar coincident with high-energy neutrino IceCube-170922A. Science, 361:eaat1378, 2018. doi: 10.1126/science.aat1378.
- [20] The ANTARES Neutrino Telescope. The Astrophysical Journal, 2015. doi: 10.48550/arXiv.1505.00224.
- [21] M. G. Aartsen et al. First observation of pev-energy neutrinos with icecube. Physical Review Letters, 111(2), July 2013. ISSN 1079-7114. doi: 10.1103/physrevlett.111.021103. URL <http://dx.doi.org/10.1103/PhysRevLett.111.021103>.
- [22] M.G. Aartsen et al. Flavor ratio of astrophysical neutrinos above 35 tev in icecube. Physical Review Letters, 114(17), April 2015. ISSN 1079-7114. doi: 10.1103/physrevlett.114.171102. URL <http://dx.doi.org/10.1103/PhysRevLett.114.171102>.
- [23] Francis Halzen. Icecube: Neutrinos from active galaxies, 2023.
- [24] A. Albert et al. Antares neutrino search for time and space correlations with icecube high-energy neutrino events. The Astrophysical Journal, 879(2):108, July 2019. ISSN 1538-4357. doi: 10.3847/1538-4357/ab253c. URL <http://dx.doi.org/10.3847/1538-4357/ab253c>.
- [25] Christian Spiering. History of high-energy neutrino astronomy, 2019.
- [26] Erik Blaufuss, Thomas Kintscher, Lu Lu, and Chun Fai Tung. The next generation of icecube realtime neutrino alerts, 2019.

- [27] S Adrián-Martínez et al. Letter of intent for km3net 2.0. *Journal of Physics G: Nuclear and Particle Physics*, 43(8):084001, June 2016. ISSN 1361-6471. doi: 10.1088/0954-3899/43/8/084001. URL <http://dx.doi.org/10.1088/0954-3899/43/8/084001>.
- [28] GVD Collaboration et. al. The baikal-gvd neutrino telescope: First results of multi-messenger studies, 2019.
- [29] Matteo Agostini et al. The pacific ocean neutrino experiment. *Nature Astronomy*, 4(10):913–915, September 2020. ISSN 2397-3366. doi: 10.1038/s41550-020-1182-4. URL <http://dx.doi.org/10.1038/s41550-020-1182-4>.
- [30] V.S. Beresinsky and G.T. Zatsepin. Cosmic rays at ultra high energies (neutrino?). *Physics Letters B*, 28(6):423–424, 1969. ISSN 0370-2693. doi: [https://doi.org/10.1016/0370-2693\(69\)90341-4](https://doi.org/10.1016/0370-2693(69)90341-4). URL <https://www.sciencedirect.com/science/article/pii/0370269369903414>.
- [31] T. Heibges et al. Overview of the EUSO-SPB2 Target of Opportunity program using the Cherenkov Telescope. In *36th International Cosmic Ray Conference (ICRC2023)*, volume 38 of *International Cosmic Ray Conference*, 2023.
- [32] Tonia M. Venters, Mary Hall Reno, John F. Krizmanic, Luis A. Anchordoqui, Claire Guépin, and Angela V. Olinto. POEMMA’s Target of Opportunity Sensitivity to Cosmic Neutrino Transient Sources. *Phys. Rev. D*, 102:123013, 2020. doi: 10.1103/PhysRevD.102.123013.
- [33] Ke Fang and Brian D. Metzger. High-Energy Neutrinos from Millisecond Magnetars Formed From the Merger of Binary Neutron Stars. *The Astrophysical Journal*, 849, 2017. doi: 10.3847/1538-4357/aa8b6a.
- [34] Cecilia Lunardini and Walter Winter. High energy neutrinos from the tidal disruption of stars. *Phys. Rev. D*, 95:123001, 2017. doi: 10.1103/PhysRevD.95.123001.
- [35] Lixin Dai and Ke Fang. Can tidal disruption events produce the IceCube neutrinos? *Monthly Notices of the Royal Astronomical Society*, 469:1354, 2017. doi: 10.1093/mnras/stx863.
- [36] Murase, Oikonomou, and Petropoulou. Blazar Flares as an Origin of High-energy Cosmic Neutrinos? *The Astrophysical Journal*, 865, 2018. doi: 10.3847/1538-4357/aada00.
- [37] Xavier Rodrigues et al. Neutrinos and Ultra-high-energy Cosmic-ray Nuclei from Blazars. *The Astrophysical Journal*, 854:54, 2018. doi: 10.3847/1538-4357/aaa7ee.
- [38] Kumiko Kotera and Joseph Silk. Ultrahigh-Energy Cosmic Rays and Black Hole Mergers. *The Astrophysical Journal Letters*, 823:L29, 2016. doi: 10.3847/2041-8205/823/2/L29.
- [39] Eli Waxman and John Bahcall. High Energy Neutrinos from Cosmological Gamma-Ray Burst Fireballs. *Physical Review Letters*, 78:2292, 1997. doi: 10.1103/PhysRevLett.78.2292.
- [40] Shigeo S. Kimura, Kohta Murase, Peter Mészáros, and Kenta Kiuchi. High-energy Neutrino Emission from Short Gamma-Ray Bursts: Prospects for Coincident Detection with Gravitational Waves. *The Astrophysical Journal Letters*, 848:L4, 2017. doi: 10.3847/2041-8213/aa8d14.
- [41] Claire Guépin, Kumiko Kotera, and Foteini Oikonomou. High-energy neutrino transients and the future of multi-messenger astronomy. *Nature Rev. Phys.*, 4(11):697–712, 2022. doi: 10.1038/s42254-022-00504-9.

- [42] J. Posligua et al. Neutrino Target of Opportunity Sky Coverage and Scheduler for EUSO-SPB2. PoS, ICRC2023:1038, 2023. doi: 10.22323/1.444.1038.
- [43] T. Heibges et al. Overview of the EUSO-SPB2 Target of Opportunity program using the Cherenkov Telescope. PoS, ICRC2023:1134, 2023. doi: 10.22323/1.444.1134.
- [44] Melinder, Dahlen, and others. The rate of supernovae at redshift 0.1–1.0. Astronomy Astrophysics, 545:A96, 2012. doi: 10.1051/0004-6361/201219364.
- [45] B.P. Abbott et al. Observation of gravitational waves from a binary black hole merger. Physical Review Letters, 116(6), February 2016. ISSN 1079-7114. doi: 10.1103/physrevlett.116.061102. URL <http://dx.doi.org/10.1103/PhysRevLett.116.061102>.
- [46] Riccardo Sturani. Gravitational waves and neutrinos, 2018.
- [47] M.G. Aartsen et al. Observation of high-energy astrophysical neutrinos in three years of icecube data. Physical Review Letters, 113(10), September 2014. ISSN 1079-7114. doi: 10.1103/physrevlett.113.101101. URL <http://dx.doi.org/10.1103/PhysRevLett.113.101101>.
- [48] Edo Berger. Short-duration gamma-ray bursts. Annual Review of Astronomy and Astrophysics, 52(1): 43–105, August 2014. ISSN 1545-4282. doi: 10.1146/annurev-astro-081913-035926. URL <http://dx.doi.org/10.1146/annurev-astro-081913-035926>.
- [49] A. Albert et al. Search for high-energy neutrinos from binary neutron star merger gw170817 with antares, icecube, and the pierre auger observatory. The Astrophysical Journal, 850(2):L35, November 2017. ISSN 2041-8213. doi: 10.3847/2041-8213/aa9aed. URL <http://dx.doi.org/10.3847/2041-8213/aa9aed>.
- [50] Stefano Bagnasco. The ligo-virgo-kagra computing infrastructure for gravitational-wave research, 2023.

APPENDIX A
SHUTTER TILT SYSTEM OPERATION MANUAL

Welcome to the ST Operation Guide!

Here you will find information on, commanding the ST, the ST status package, troubleshooting and expert information.

A.1 Commanding

In a new terminal, open “STFINAL.py”.

You will be welcomed to the program and prompted to “Enter the command to send”.

```
spb2@spb2st:~/stcmd$ python3 ST_FINAL.py
Welcome to the CTSTOS - The Cherenkov Telescope Shutter/Tilt Operating System!
A list of commands and other information can be found by entering 'Help' below.
Happy Operating!
*****
Enter the command to send: 
```

Figure A.1 The ST manual welcome prompt

If you know the command you would like to send, go ahead and enter it. Otherwise, you can type “help” (NOT case-sensitive) to get a list of commands (also included below).

```
Enter the command to send: help
Note: commands are case sensitive

Close          close the CT shutters
Timed Open     open the shutters for a specified amount of minutes
Tilt           tilt the CT a specific angle change, enter the angle change (+ i
Status         retrieve most recent status of ST system from UAH server (status
TiltAll Up     tilt the CT from its lower limit to its upper limit
TiltAll Down   tilt the CT from its upper limit to its lower limit
TiltDeg Up     tilt the CT 1 degree upward
TiltDeg Down   tilt the CT 1 degree downward
Get Config     get the current ST system configuration, including motor speeds

**WARNING**    If there is a mechanical error, DO NOT send more commands
               Instead, power cycle the ST system. This power cycle stop the ti
               The shutters will close when power is restored.

Enter 'expert' for expert help
*****
Enter the command to send: 
```

Figure A.2 ST user commands

*Note: Commands are case-sensitive

*Note: To open the shutters, you must specify the amount of time for the shutters to remain open in minutes. After this time, the shutters will close automatically. If you send a “Close” command before this

time is up, the shutters will close and this time will be overwritten

A.1.1 Timing of the ST

Table A.1 Timing of the ST

<i>Action</i>	<i>Time</i>
Tilt 1 Degree	5 minutes
Tilt from limit to limit	30 minutes
Open Shutters	2 minutes
Close Shutters	2 minutes

For larger moves, you can check that the command went through by getting a status about a minute in and checking that the motor has been energized.

A.2 Status Package

The status package for the ST system is 15 bytes. You will interact with the status package either in Grafana or in the command line of the commanding program.

A.2.1 Grafana User Interface

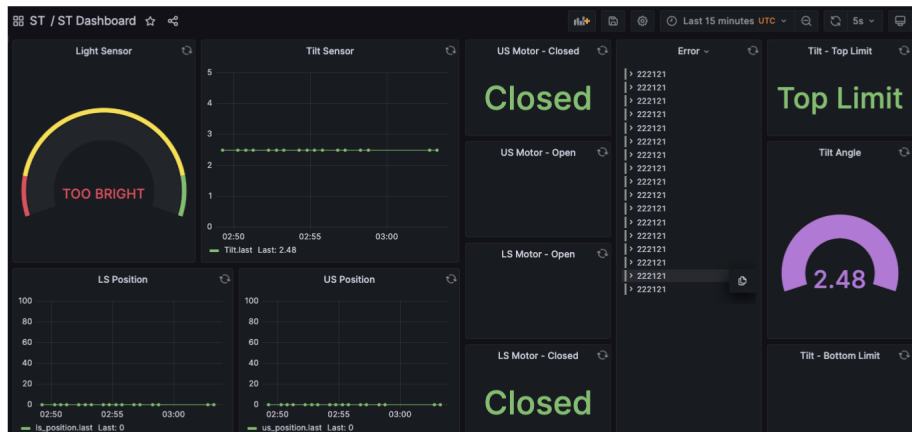


Figure A.3 Grafana user interface

A.2.2 Command Line

If using the command line, there are two commands you can use to retrieve the status: "Status" and "Full Status"

If you use the command "status", you will receive the status in an easy-to-read format which includes the time stamp, the status bytes, the status of the shutter and tilt motors, the angle of the CT

inclinometer, and the value of the CT light sensor. This information will be displayed as follows:

Table A.2 ST status headers

ST Status @ time stamp (year-month-day hour-minute-seconds)

Upper Shutter:

Lower Shutter:

Tilt:

Angle:

Light:

```
.....
Enter the command to send: status
ST Status @ 2023-04-28 03:02:47
22212104d800000000027b9ec70000

Upper Shutter: Closed/Motor Stopped

Lower Shutter: Closed/Motor Stopped

Tilt: Motor Stopped/Top Limit Activated
Angle: 2.48 degrees +/- 0.12 (maximum is +3.5/-15)

Light: 0 (max brightness = 0, minimum brightness = 15)
**WARNING** TOO BRIGHT! DO NOT OPEN SHUTTERS! **WARNING**
*****
Enter the command to send: 
```

Figure A.4 ST status message

A.3 Troubleshooting and Expert Information

If you are an expert, you can see a list of expert commands (also included below) by typing “expert” into the command prompt.

About the mechanical error warning below the commands box: If there is a mechanical error, the motors will not stop spinning until: they hit a limit switch; they burn out; power is cut.

If it is unclear whether hitting the limit switch is possible or will help, and with the intention of avoiding number 2 on that list, the best option is to power cycle the PLC. This will terminate all motion in the ST system. Do not wait to do this until the driver boards or motors themselves burn out.

A mechanical error could be indicated by: A limit switch doesn’t trip (upper or lower) A list of limits will be included in the troubleshooting section below This could mean the Shutters are slamming into the CT frame, or opening further than they should, which could cause clearance issues with the solar frame This could also mean the tilt system is moving further up or down than it should, which could cause clearance issues with the solar frame or unexpected tension on CT cables A motor that stays “energized” This could mean the motors are continuing to spin, even if the shutters or tilt have been stopped by a limit

switch This could also mean the motors are trying to move the system, but the shutters are not opening or closing properly (not moving at all) or the tilt system is stuck

A.3.1 Expert Commands

*Note: Commands are case-sensitive

```

Enter the command to send: expert
*****
Welcome, expert operator!

Here is a list of commands you may find useful as an expert operator:
Note: commands are case sensitive

Open                open the CT shutters for an indefinite amount of time
Configure this device  configure the device, including motor speeds, shutter limits, and max timeout
Full Status          retrieve the full status of the device, including shutter positions device configuration, and the number of
                    steps needed to completely open or completely close the shutters
Shutter Steps        move the shutters individually, provided a number of steps in decimal
Single Shutter Open  completely open one shutter at a time
Single Shutter Close completely close one shutter at a time

Enter 'help' for non-expert commands
*****
Enter the command to send: 

```

Figure A.5 ST expert commands

A.3.2 Limits

The limits of movement for each system of the S/T are below.

Table A.3 ST limits

<i>System</i>	<i>Limit</i>	<i>Value</i>
Tilt	Upper limit	2.5 degrees above horizontal
Tilt	Lower Limit	13.09 degrees below horizontal
Lower Shutter	Open Limit	
Upper Shutter	Open Limit	

A.3.3 "Full Status" and Device Configuration

The 15 byte device configuration represents CCXXVVVVVVVVVVVVVVVMMMMMMMTTTTAA

A.3.4 Status Bytes

The 15 byte status message represents:

A.3.5 System Specs

Table A.4 Device configuration status

<i>Byte</i>	<i>What's Represented</i>	<i>Bit Assignments</i>
1 byte (CC)	Identification	Identifies this status as the configuration
1 byte (XX)	Reserved	Reserved
2 bytes	Tilt motor speed	16 bits (8 hex digits) representing the operation speed for the tilt motor, in units of full steps per second. Default is 425 steps per second. PLC imposes hard limit of 600 decimal (equivalent to 3 rps)
2 bytes	Lower shutter motor speed	16 bits (8 hex digits) representing the operation speed for the lower shutter motor, in units of full steps per second. Default is 300 steps per second. PLC imposes hard limit of 600 decimal (equivalent to 3 rps)
2 bytes	Upper shutter motor speed	16 bits (8 hex digits) representing the operation speed for the lower shutter motor, in units of full steps per second. Default is 300 steps per second. PLC imposes hard limit of 600 decimal (equivalent to 3 rps)
2 bytes	Lower shutter max steps	16 bits (8 hex digits) representing the max movement steps for the lower shutter. Default is 8000 steps
2 bytes	Upper shutter max steps	16 bits (8 hex digits) representing the max movement steps for the upper shutter. Default is 8000 steps
2 bytes	Max timeout	16 bits (8 hex digits) representing the maximum shutter timeout in minutes. Default is 480 minutes (8 hours)
1 byte	Available	Available

Table A.5 Status message

Byte	What's Represented	Bit Assignments
1 byte	Tilt motor	<ol style="list-style-type: none"> 1. Lower Limit Switch is closed 2. Upper Limit Switch is closed 3. Reserved for software position limits 4. Reserved for software position limits 5. Motor is energized 6. Motor is stopped 7. Axis has been homed 8. MSB: Error
1 byte	Lower shutter motor	<ol style="list-style-type: none"> 1. Lower Limit Switch is closed 2. Upper Limit Switch is closed 3. Reserved for software position limits 4. Reserved for software position limits 5. Motor is energized 6. Motor is stopped 7. Axis has been homed 8. MSB: Error
1 byte	Upper shutter motor	<ol style="list-style-type: none"> 1. Lower Limit Switch is closed 2. Upper Limit Switch is closed 3. Reserved for software position limits 4. Reserved for software position limits 5. Motor is energized 6. Motor is stopped 7. Axis has been homed 8. MSB: Error
1 Nibble ($\frac{1}{2}$ a byte)	Light sensor	4 bits (1 hex digit) representing integers 0 to 15 in which lower values represent more light
3 Nibbles ($1\frac{1}{2}$ bytes)	Tilt sensor	Tilt angle measured by the inclinometer. 12 bits (3 hex digits) representing integers 0 to 4095 mapping to the 0 – 10V output range of the inclinometer
2 bytes	Lower shutter position	The current position in whole steps (not microsteps). 16 bits (4 hex digits) representing integers -32768 to +32767 steps
2 bytes	Upper shutter position	The current position in whole steps (not microsteps). 16 bits (4 hex digits) representing integers -32768 to +32767 steps
4 bytes	Timestamp	Seconds passed since Jan 1, 2022 UTC time
2 bytes	Minutes until shutters close	Minutes remaining until shutter automatically closes (after a “Timed Open” command)

Table A.6 System specs

Item	Description	Notes
Controller	Siemens PLC 6AG12141AG402XB0	
Stepper Drivers	2A@24V	identical for all 3 motors
Motors	Stepper motors, Vacuum rated	Empire Magnetics U31 for Tilt
Tilting	~+3 to ~-15 elevation angle relative to horizontal	411904 steps total 38842 steps (97BA hex)/degree ~43 sec/degree 1.64 cm/degree
Tilting - weight to lift	286 lbs straight up	
Tilting - linear stage	Thompson	ball screw low temp lubricant
Light sensor	1 light-sensitive resistor	read out by PLC
Inclinometer	1 Reiker H6MM Data package changes by 34.3 decimal per degree A 1 decimal change in the package represents a degree change of 0.0291 deg 0 deg = 1153 decimal = 481	approx. 0.1 deg accuracy, read out by PLC
System power draw	Tilt motor: 24 W/12.96 W/5.52 W Upper shutter motor: 31.2 W/21.36 W/5.52 W Lower shutter motor: 33.6 W/21.36W/5.52 W	Speeding up or down/while running/idle
System current draw	Tilt motor: 1 A/0.54 A/0.23 A Upper shutter motor: 1.3 A/0.89 A/0.23 A Lower shutter motor: 1.4 A/0.89 A/0.23 A	Speeding up or down/while running/idle

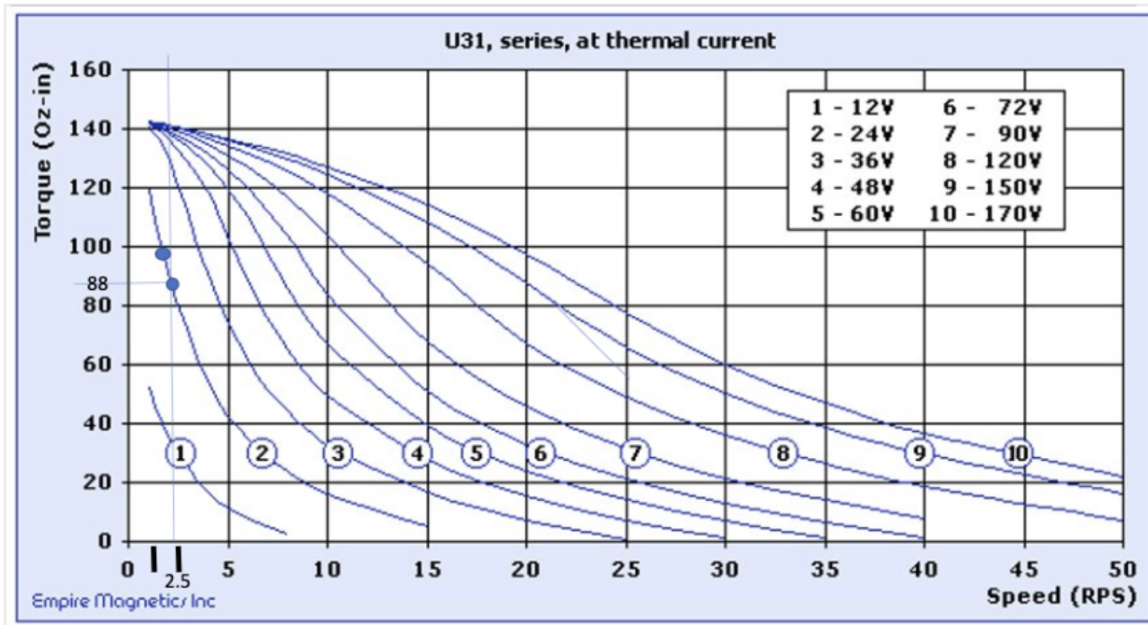


Figure A.6 Shutter stepper motor specs

Speed (RPS)	Torque (oz-in)									
	12 V	24 V	36 V	48 V	60 V	72 V	90 V	120 V	150 V	170 V
1	52	119	140	142	142	142	143	143	143	143
2	35	91	131	137	139	140	140	141	141	141
4	17	54	91	119	128	132	135	137	138	138
6	8	35	62	88	110	120	127	132	134	135
8	3	24	44	65	86	104	117	126	130	131
10	N/A	16	33	50	67	84	104	118	125	127
15	N/A	5	16	28	39	51	68	94	108	114
20	N/A	N/A	7	16	24	33	46	67	88	97
25	N/A	N/A	0	7	14	21	32	49	66	78
30	N/A	N/A	N/A	1	7	13	21	36	50	60
35	N/A	N/A	N/A	N/A	2	6	14	26	39	47
40	N/A	N/A	N/A	N/A	N/A	1	8	19	29	37
50	N/A	N/A	N/A	N/A	N/A	N/A	N/A	7	16	22

Figure A.7 Shutter stepper motor specs

APPENDIX B

ALL SOURCES OBSERVABLE ON MAY 14TH, 2023

Name	Type	Tier	Start Time	End Time	Start Location	End Location	Pointing Direction
SN 2023ftg	SN II	inf	2023-05-14T06:25:30.000	2023-05-14T06:45:30.000	(-10.02 82.39)	(-5.51 79.60)	(-9.00 81.69)
SN 2023gjjg	SN II	inf	2023-05-14T08:25:30.000	2023-05-14T08:55:30.000	(-7.60 309.95)	(-13.04 306.33)	(-9.00 308.73)
SN 2023fwr	SN Ic	6	2023-05-14T06:05:30.000	2023-05-14T06:35:30.000	(-10.66 47.71)	(-5.79 44.08)	(-9.00 46.52)
SN 2023hcp	SN II	inf	2023-05-14T06:05:30.000	2023-05-14T06:35:30.000	(-11.15 54.40)	(-5.76 50.70)	(-9.00 53.19)
SN 2023hlf	SN II	inf	2023-05-15T08:35:30.000	2023-05-15T08:55:30.000	(-6.95 304.42)	(-10.83 301.20)	(-9.00 303.61)
AT 2023elx	TDE	3	2023-05-15T08:45:30.000	2023-05-15T08:55:30.000	(-7.37 283.57)	(-9.62 281.83)	(-9.00 283.57)
AT 2022wtn	TDE	inf	2023-05-15T08:25:30.000	2023-05-15T08:45:30.000	(-9.92 83.97)	(-5.33 80.43)	(-9.00 83.09)
AT 2022upj	TDE	inf	2023-05-15T07:55:30.000	2023-05-15T08:25:30.000	(-11.97 119.14)	(-5.76 113.21)	(-9.00 117.14)
None	GRB	inf	2023-05-15T07:45:30.000	2023-05-15T08:25:30.000	(-6.28 318.30)	(-12.78 312.14)	(-9.00 315.96)
None	GRB	inf	2023-05-14T10:15:30.000	2023-05-14T10:55:30.000	(-6.12 222.30)	(-11.75 215.27)	(-9.00 219.71)
None	GRB	inf	2023-05-14T09:15:30.000	2023-05-14T10:55:30.000	(-6.16 194.63)	(-8.21 176.85)	(-9.00 188.23)
None		3	2023-05-14T10:15:30.000	2023-05-14T10:45:30.000	(-7.29 316.47)	(-12.19 312.87)	(-9.00 315.25)
None	GRB	inf	2023-05-14T08:15:30.000	2023-05-14T08:35:30.000	(-9.91 71.97)	(-5.63 69.27)	(-9.00 71.30)
None	Swift-FOM	inf	2023-05-14T07:45:30.000	2023-05-14T08:25:30.000	(-7.17 319.93)	(-13.42 315.31)	(-9.00 318.17)
None	GRB	inf	2023-05-14T07:45:30.000	2023-05-14T08:25:30.000	(-6.29 317.71)	(-12.79 312.95)	(-9.00 315.90)
4FGL J0910.0+4257	AGN	4	2023-05-14T08:05:30.000	2023-05-14T08:35:30.000	(-7.15 317.08)	(-12.03 313.51)	(-9.00 315.87)
SDSS J102906.69+555625.2	AGN	4	2023-05-14T05:15:30.000	2023-05-14T05:35:30.000	(-7.87 47.75)	(-4.51 45.20)	(-9.00 47.12)
PMN J1913-3630	blazar	4	2023-05-14T05:15:30.000	2023-05-14T05:25:30.000	(-6.73 141.53)	(-5.32 139.91)	(-9.00 141.53)
PMN J1913-3630	blazar	4	2023-05-14T05:15:30.000	2023-05-14T05:25:30.000	(-6.73 141.53)	(-5.32 139.91)	(-9.00 141.53)
Old TA Hotspot	Steady hotspot	8	2023-05-14T08:35:30.000	2023-05-14T09:15:30.000	(-6.62 314.46)	(-13.47 309.67)	(-9.00 312.63)
NGC 253	Steady Seyfert	8	2023-05-14T10:45:30.000	2023-05-14T10:55:30.000	(-11.15 130.12)	(-9.37 128.39)	(-9.00 130.12)
Mrk 421	Steady Blazar	8	2023-05-14T10:05:30.000	2023-05-14T10:35:30.000	(-6.80 311.50)	(-12.10 307.79)	(-9.00 310.25)
Mrk 501	Steady Blazar	8	2023-05-14T06:25:30.000	2023-05-14T06:55:30.000	(-10.50 49.35)	(-5.50 45.67)	(-9.00 48.15)
BL Lacertae	Steady Blazar	8	2023-05-15T08:45:30.000	2023-05-15T08:55:30.000	(-11.44 44.36)	(-9.83 42.86)	(-9.00 44.36)
PKS 2155-304	Steady HBL	8	2023-05-14T07:45:30.000	2023-05-14T08:25:30.000	(-11.88 137.86)	(-5.28 131.08)	(-9.00 135.28)
1ES 1218+304	Steady HBL	8	2023-05-15T08:35:30.000	2023-05-15T08:55:30.000	(-7.10 302.93)	(-11.04 299.69)	(-9.00 302.11)
H 2356-309	Steady HBL	8	2023-05-14T09:35:30.000	2023-05-14T10:15:30.000	(-11.50 138.33)	(-4.98 131.52)	(-9.00 135.74)
PKS 0548-322	Steady HBL	8	2023-05-14T08:35:30.000	2023-05-14T09:15:30.000	(-6.98 224.19)	(-12.84 217.11)	(-9.00 221.58)
1ES 0347-121	Steady HBL	8	2023-05-14T05:35:30.000	2023-05-14T06:05:30.000	(-7.31 250.91)	(-13.70 246.15)	(-9.00 249.35)
1ES 1011+496	Steady HBL	8	2023-05-14T08:35:30.000	2023-05-14T09:15:30.000	(-7.16 325.80)	(-12.67 321.21)	(-9.00 324.05)
1ES 0806+524	Steady HBL	8	2023-05-14T06:25:30.000	2023-05-14T07:05:30.000	(-7.09 329.71)	(-12.13 325.22)	(-9.00 328.00)
RGB J0710+591	Steady HBL	8	2023-05-14T05:15:30.000	2023-05-14T05:35:30.000	(-10.66 336.12)	(-12.50 334.10)	(-9.00 335.61)
1ES 0414+009	Steady HBL	8	2023-05-14T05:25:30.000	2023-05-14T05:55:30.000	(-6.60 267.17)	(-13.41 262.78)	(-9.00 265.72)
PKS 0447-439	Steady HBL	8	2023-05-14T08:45:30.000	2023-05-14T10:05:30.000	(-6.47 205.84)	(-12.08 191.17)	(-9.00 199.47)
SHBL J001355.9-185406	Steady HBL	8	2023-05-14T10:35:30.000	2023-05-14T10:55:30.000	(-11.65 121.66)	(-7.69 118.33)	(-9.00 120.82)
RX J0648.7+1516	Steady HBL	8	2023-05-14T07:15:30.000	2023-05-14T07:45:30.000	(-7.10 283.58)	(-13.83 279.46)	(-9.00 282.20)
HESS J1943+213	Steady HBL	8	2023-05-14T08:15:30.000	2023-05-14T08:35:30.000	(-10.26 71.13)	(-6.00 68.44)	(-9.00 70.46)
1ES 1215+303	Steady HBL	8	2023-05-15T08:35:30.000	2023-05-15T08:55:30.000	(-7.64 302.35)	(-11.61 299.13)	(-9.00 301.54)
1ES 1741+196	Steady HBL	8	2023-05-14T06:15:30.000	2023-05-14T06:45:30.000	(-11.23 73.86)	(-4.73 69.84)	(-9.00 72.53)

Figure B.1 All the sources in the ToO source catalog the night of May 14th 2023

[Figure B.1 continued]

1ES 1741+196	Steady HBL	8	2023-05-14T06:15:30.000	2023-05-14T06:45:30.000	(-11.23 73.86)	(-4.73 69.84)	(-9.00 72.53)
1ES 1727+502	Steady HBL	8	2023-05-14T07:35:30.000	2023-05-14T08:15:30.000	(-10.85 36.38)	(-5.84 31.67)	(-9.00 34.65)
KUV 00311-1938	Steady HBL	8	2023-05-15T07:45:30.000	2023-05-15T08:25:30.000	(-11.94 126.40)	(-4.15 118.43)	(-9.00 123.38)
PKS 0301-243	Steady HBL	8	2023-05-14T05:25:30.000	2023-05-14T05:55:30.000	(-6.59 236.07)	(-12.16 231.12)	(-9.00 234.45)
H 1722+119	Steady HBL	8	2023-05-14T05:45:30.000	2023-05-14T06:05:30.000	(-10.10 82.28)	(-5.59 79.51)	(-9.00 81.59)
RBS 0723	Steady HBL	8	2023-05-14T09:15:30.000	2023-05-14T09:35:30.000	(-7.56 278.81)	(-12.09 275.97)	(-9.00 278.10)
RGB J2243+203	Steady HBL	8	2023-05-15T08:15:30.000	2023-05-15T08:35:30.000	(-10.36 72.08)	(-5.99 68.67)	(-9.00 71.23)
1ES 2037+521	Steady HBL	8	2023-05-14T10:45:30.000	2023-05-14T10:55:30.000	(-10.94 33.22)	(-9.73 32.10)	(-9.00 33.22)
PGC 2402248	Steady HBL	8	2023-05-14T05:45:30.000	2023-05-14T06:35:30.000	(-6.08 330.18)	(-12.30 324.51)	(-9.00 327.88)
1ES 2322-409	Steady HBL	8	2023-05-14T07:55:30.000	2023-05-14T08:55:30.000	(-11.67 156.72)	(-4.96 146.17)	(-9.00 152.27)
1ES 0647+250	Steady HBL	8	2023-05-14T06:55:30.000	2023-05-14T07:25:30.000	(-7.52 294.92)	(-13.87 291.06)	(-9.00 293.62)
RX J1136.5+6737	Steady HBL	8	2023-05-14T05:15:30.000	2023-05-14T07:55:30.000	(-10.52 5.99)	(-12.16 349.53)	(-9.00 359.59)
1RXS J023832.6-311658	Steady HBL	8	2023-05-14T05:35:30.000	2023-05-14T06:05:30.000	(-7.62 225.41)	(-12.33 220.23)	(-9.00 223.71)
1RXS J081201.8+023735	Steady HBL	8	2023-05-14T09:05:30.000	2023-05-14T09:25:30.000	(-7.92 267.95)	(-12.46 264.96)	(-9.00 267.21)
MRC 0910-208	Steady HBL	8	2023-05-15T08:25:30.000	2023-05-15T08:55:30.000	(-7.30 235.77)	(-12.85 229.59)	(-9.00 233.74)
1RXS J195815.6-301119	Steady HBL	8	2023-05-14T05:55:30.000	2023-05-14T06:35:30.000	(-11.88 137.58)	(-5.26 130.85)	(-9.00 135.02)
RGB J2042+244	Steady HBL	8	2023-05-14T09:15:30.000	2023-05-14T09:45:30.000	(-10.62 67.57)	(-4.43 63.55)	(-9.00 66.24)
W Comae	Steady IBL	8	2023-05-15T08:45:30.000	2023-05-15T08:55:30.000	(-7.80 299.77)	(-9.82 298.13)	(-9.00 299.77)
MAGIC J2001+435	Steady IBL	8	2023-05-14T09:35:30.000	2023-05-14T10:05:30.000	(-10.47 43.92)	(-5.95 40.25)	(-9.00 42.71)
VER J0521+211	Steady IBL	8	2023-05-14T05:45:30.000	2023-05-14T06:05:30.000	(-8.09 290.05)	(-12.39 287.45)	(-9.00 289.39)
B2 1811+31	Steady IBL	8	2023-05-14T07:15:30.000	2023-05-14T07:45:30.000	(-10.71 59.06)	(-5.00 55.23)	(-9.00 57.80)

[Figure B.1 continued]

B2 1811+31	Steady IBL	8	2023-05-14T07:15:30.000	2023-05-14T07:45:30.000	(-10.71 59.06)	(-5.00 55.23)	(-9.00 57.80)
OT 081	Steady LBL	8	2023-05-14T06:05:30.000	2023-05-14T06:25:30.000	(-9.99 84.83)	(-5.45 82.03)	(-9.00 84.13)
PKS 0736+017	Steady FSRQ	8	2023-05-14T08:35:30.000	2023-05-14T09:05:30.000	(-7.43 267.06)	(-14.23 262.54)	(-9.00 265.57)
TON 0599	Steady FSRQ	8	2023-05-15T08:15:30.000	2023-05-15T08:45:30.000	(-6.24 302.43)	(-12.23 297.56)	(-9.00 300.79)
PKS 0346-27	Steady FSRQ	8	2023-05-14T06:25:30.000	2023-05-14T06:55:30.000	(-7.49 230.36)	(-12.51 225.19)	(-9.00 228.66)
3C 264	Steady FRI	8	2023-05-15T08:35:30.000	2023-05-15T08:55:30.000	(-6.84 289.43)	(-11.24 286.03)	(-9.00 288.58)
FRB 20190208A	Steady FRB	8	2023-05-14T08:35:30.000	2023-05-14T09:25:30.000	(-11.82 41.10)	(-4.89 35.09)	(-9.00 38.74)
FRB 20190417A	Steady FRB	8	2023-05-14T10:25:30.000	2023-05-14T10:55:30.000	(-11.86 24.29)	(-9.29 21.05)	(-9.00 23.23)
FRB 20181119A	Steady FRB	8	2023-05-14T05:15:30.000	2023-05-14T09:35:30.000	(-10.47 13.10)	(-12.29 344.41)	(-9.00 6.70)
FRB 20180301A	Steady FRB	8	2023-05-14T07:05:30.000	2023-05-14T07:35:30.000	(-6.75 271.13)	(-13.60 266.73)	(-9.00 269.67)
FRB 20190303A	Steady FRB	8	2023-05-15T08:25:30.000	2023-05-15T08:55:30.000	(-6.36 329.61)	(-10.07 325.02)	(-9.00 328.06)
FRB 20200120E	Steady FRB	8	2023-05-14T05:15:30.000	2023-05-14T06:05:30.000	(-11.28 356.70)	(-12.24 351.86)	(-9.00 354.76)
FRB 20201124A	Steady FRB	8	2023-05-14T05:15:30.000	2023-05-14T05:45:30.000	(-7.11 296.46)	(-13.26 292.68)	(-9.00 295.19)
FRB 20121102A	Steady FRB	8	2023-05-14T05:15:30.000	2023-05-14T05:45:30.000	(-6.60 305.28)	(-12.22 301.61)	(-9.00 304.03)
Cygnus Cocoon	Steady cloud	8	2023-05-14T09:45:30.000	2023-05-14T10:25:30.000	(-11.46 47.96)	(-5.04 43.01)	(-9.00 46.13)
Crab Nebula	Steady PWN	8	2023-05-14T05:45:30.000	2023-05-14T06:15:30.000	(-6.08 292.30)	(-12.49 288.37)	(-9.00 290.98)
LHAASO J1825-1326	Steady	8	2023-05-14T05:35:30.000	2023-05-14T06:05:30.000	(-10.99 113.73)	(-4.66 109.07)	(-9.00 112.16)
LHAASO J1839-0545	Steady	8	2023-05-14T06:05:30.000	2023-05-14T06:35:30.000	(-11.87 104.64)	(-5.14 100.10)	(-9.00 103.11)
LHAASO J1843-0338	Steady	8	2023-05-14T06:15:30.000	2023-05-14T06:45:30.000	(-11.47 101.78)	(-4.69 97.29)	(-9.00 100.27)
LHAASO J1849-0003	Steady	8	2023-05-14T06:35:30.000	2023-05-14T06:55:30.000	(-10.25 96.59)	(-5.69 93.65)	(-9.00 95.85)
LHAASO J1908+0621	Steady	8	2023-05-14T07:05:30.000	2023-05-14T07:35:30.000	(-10.78 89.23)	(-3.94 84.94)	(-9.00 87.80)

[Figure B.1 continued]

3C 264	Steady FRI	8	2023-05-15T08:35:30.000	2023-05-15T08:55:30.000	(-6.84 289.43)	(-11.24 286.03)	(-9.00 288.58)
FRB 20190208A	Steady FRB	8	2023-05-14T08:35:30.000	2023-05-14T09:25:30.000	(-11.82 41.10)	(-4.89 35.09)	(-9.00 38.74)
FRB 20190417A	Steady FRB	8	2023-05-14T10:25:30.000	2023-05-14T10:55:30.000	(-11.86 24.29)	(-9.29 21.05)	(-9.00 23.23)
FRB 20181119A	Steady FRB	8	2023-05-14T05:15:30.000	2023-05-14T09:35:30.000	(-10.47 13.10)	(-12.29 344.41)	(-9.00 6.70)
FRB 20180301A	Steady FRB	8	2023-05-14T07:05:30.000	2023-05-14T07:35:30.000	(-6.75 271.13)	(-13.60 266.73)	(-9.00 269.67)
FRB 20190303A	Steady FRB	8	2023-05-15T08:25:30.000	2023-05-15T08:55:30.000	(-6.36 329.61)	(-10.07 325.02)	(-9.00 328.06)
FRB 20200120E	Steady FRB	8	2023-05-14T05:15:30.000	2023-05-14T06:05:30.000	(-11.28 356.70)	(-12.24 351.86)	(-9.00 354.76)
FRB 20201124A	Steady FRB	8	2023-05-14T05:15:30.000	2023-05-14T05:45:30.000	(-7.11 296.46)	(-13.26 292.68)	(-9.00 295.19)
FRB 20121102A	Steady FRB	8	2023-05-14T05:15:30.000	2023-05-14T05:45:30.000	(-6.60 305.28)	(-12.22 301.61)	(-9.00 304.03)
Cygnus Cocoon	Steady cloud	8	2023-05-14T09:45:30.000	2023-05-14T10:25:30.000	(-11.46 47.96)	(-5.04 43.01)	(-9.00 46.13)
Crab Nebula	Steady PWN	8	2023-05-14T05:45:30.000	2023-05-14T06:15:30.000	(-6.08 292.30)	(-12.49 288.37)	(-9.00 290.98)
LHAASO J1825-1326	Steady	8	2023-05-14T05:35:30.000	2023-05-14T06:05:30.000	(-10.99 113.73)	(-4.66 109.07)	(-9.00 112.16)
LHAASO J1839-0545	Steady	8	2023-05-14T06:05:30.000	2023-05-14T06:35:30.000	(-11.87 104.64)	(-5.14 100.10)	(-9.00 103.11)
LHAASO J1843-0338	Steady	8	2023-05-14T06:15:30.000	2023-05-14T06:45:30.000	(-11.47 101.78)	(-4.69 97.29)	(-9.00 100.27)
LHAASO J1849-0003	Steady	8	2023-05-14T06:35:30.000	2023-05-14T06:55:30.000	(-10.25 96.59)	(-5.69 93.65)	(-9.00 95.85)
LHAASO J1908+0621	Steady	8	2023-05-14T07:05:30.000	2023-05-14T07:35:30.000	(-10.78 89.23)	(-3.94 84.94)	(-9.00 87.80)
LHAASO J1929+1745	Steady	8	2023-05-14T07:45:30.000	2023-05-14T08:15:30.000	(-11.97 76.39)	(-5.40 72.31)	(-9.00 75.04)
LHAASO J1956+2845	Steady	8	2023-05-14T08:45:30.000	2023-05-14T09:15:30.000	(-10.26 62.25)	(-4.36 58.30)	(-9.00 60.95)
LHAASO J2018+3651	Steady	8	2023-05-14T09:25:30.000	2023-05-14T09:55:30.000	(-11.00 52.94)	(-5.73 49.18)	(-9.00 51.71)
LHAASO J2032+4102	Steady	8	2023-05-14T09:45:30.000	2023-05-14T10:25:30.000	(-11.95 48.44)	(-5.47 43.53)	(-9.00 46.63)
LHAASO J2108+5157	Steady	8	2023-05-15T08:45:30.000	2023-05-15T08:55:30.000	(-11.80 30.77)	(-10.63 29.36)	(-9.00 30.77)